Change Detection of Land Cover in Yangon Using Remote Sensing and Machine Learning

A Thesis Submitted to the Department of Computer Science and Communication Engineering, the Graduate School of Fundamental Science and Engineering of Waseda University

in Partial Fulfillment of the Requirements

for the Degree of Master of Engineering

July 22nd, 2019.

Nyein Soe Thwal

(5117FG26-6)

Advisor: Prof. Hiroshi Watanabe

Research guidance: Research on Audiovisual Information Processing

ACKNOWLEDGEMENTS

First and foremost, I would like to express my deepest and sincere gratitude to my research supervisor Professor Hiroshi Watanabe of Department of Computer Science and Communications Engineering, Graduate School of Fundamental Science and Engineering, Waseda University for his precious guidance and supervision. He has enlightened me with the timely suggestions and his inspiration in machine learning in our group discussions. His continuous encouragement supports for my research to a successful completion.

I owe a deep sense of gratitude to Mr. Takaaki Ishikawa for his valuable suggestions, prompt inspiration, and guidance in our image processing group discussions. Moreover, I would like to extend special thanks to Japan International Cooperation Agency (JICA) which supports the financial scholarship to study my research in Waseda University through the JDS program. I thank profusely all of my lab mates in Watanabe Lab for their help, encouragement, and kindness in the whole two years of my research.

Finally, I am extremely grateful to my parents, grandparents for their loves, prayers, and caring. I am very much thankful to Mr. Chit Myo Lwin from SEM Co., Ltd for his precious discussion, helps, supports, and encouragement during my living in Japan.

ABSTRACT

Earth science and land resource management play a vital role to develop a sustainable country, especially in developing countries. The developing countries like Myanmar have very few data on environment and urban management and face many difficulties due to poor data management. Nowadays, the satellite images and open social data are widely available for research purposes. Applying these massive data effectively and efficiently based on the actual problems offer great potential to advance the science of land cover change, climate change, and anthropogenic impacts.

Therefore, the proposed method is implemented to carry out land cover mapping and change trend detection in the study area. First, the image data from these satellites are collected by the google earth engine (GEE). Image pre-processing is also performed on this cloud-based platform. The land cover of the study area for the five years from 1987 to 2012 is classified using only Landsat images based on the NDVI range. Next, the data set is trained by random forest (RF) classifier on the GEE using additional spectral features such as NDVI, NDBI, and SRTM slopes. In 2017, not only the Landsat 8 but also Sentinel 2 and open street map (OSM) data can be used for research.

In this research, we perform feature-level fusion of two satellite sensors and also combine vector features from OSM and GPS metadata to achieve better performance. Features from the Landsat 8 are extracted by using the pixel-based classification approaches in color composite images. Object-based segmentation is operated to extract features from Sentinel-2. In GEE, the input parameter can be assigned to the RF classifiers and in this study a combination of seven input band is deployed for RF. Moreover, six different machine learning algorithms are executed to show the comparison. Finally, change detection is evaluated based on the post-classification comparison of 30-year time series data. The accuracy assessment is performed based on the confusion matrix of the classifier. We tested the validity by comparing with data set from Yangon City Development Committee (YCDC) and the true color satellite image. Our proposed method achieved overall accuracy of 96.73 % and kappa statistic of 0.952.

TABLE OF CONTENTS

LIST OF FIGURES

LIST OF TABLES

CHAPTER 1
INTRODUCTION

1.1 Background

Land cover information is one of the most important resources for human beings. Because there are only a few places on the earth as natural states that are not been affected by human intervention. Accurate and timely analysis and use of land resources plays an important role in the development of human society. Due to the rapid urbanization and human activity, the earth's surface changes dramatically on a regional and global scales with regard to the ecological, socio-economic and aesthetical influences. Therefore, land cover analysis from the surface of the earth is crucial for the whole world.

Land cover means physical information from the earth's surface such as buildings, river, fields, lake, mountains, trees, and so on. There are two primary methods to detect land cover. The first approach is to detect land cover using Global Positioning System (GPS) and the second approach is to extract land cover information from the satellite images using image processing techniques. For the reason that detection of and cover using GPS is time-consuming and costly in the survey region, most of the studies are examined on satellite image processing.

Satellite images cover wide area and data from satellite images can be quickly extracted and processed using a computer. Only with the single image taken from the satellite sensor, many useful and valuable information that are related to various applications such as land cover, air quality, disaster management, urban planning, weather forecast, etc., can be interpreted. Thus, most researches for land resource management are focused on satellite image processing.

The world is developing day by day due to the rapid globalization and the surface of the earth is also changing with the time for rapid development. Most changes are caused by artificial processes and some changes are caused by natural disasters. Land cover change detection (LCCD) becomes an important topic in the remote sensing community since it plays an important role in environmental management, natural resource management and urban management. It also effects on climate, air quality, hydrology, geography, surface temperature, and more. As a

result, LCCD turns into one of the most important global challenges as it has a positive effect on the management of natural resource on the earth's surface.

1.2 Study Area

Yangon city, the study area, is a commercial capital of Myanmar and has a population of approximately 7.36 million [1]. The area is 795 km^2 and is located in lower Myanmar along with the Yangon River between latitude 17°06' to 16°35'N and longitude 95°58' to 96°24'E, east of the Ayeyarwady River delta. Yangon has a tropical monsoon climate with three distinct seasons: summer (March to the mid-May), rainy season (mid- May to mid-October), and winter (mid-October to February).

The Government of Myanmar is moving toward democracy and rapid urbanization and accelerated development are occurring in Yangon as it is considered to be the commercial and financial hub of the country as well as the gateway to tourism. In addition, Yangon is the largest city in Myanmar, and has recorded a rapid population growth over the past ten years. The average population growth rate in Yangon between 1998 and 2011 was 2.58% annually. In the meantime,

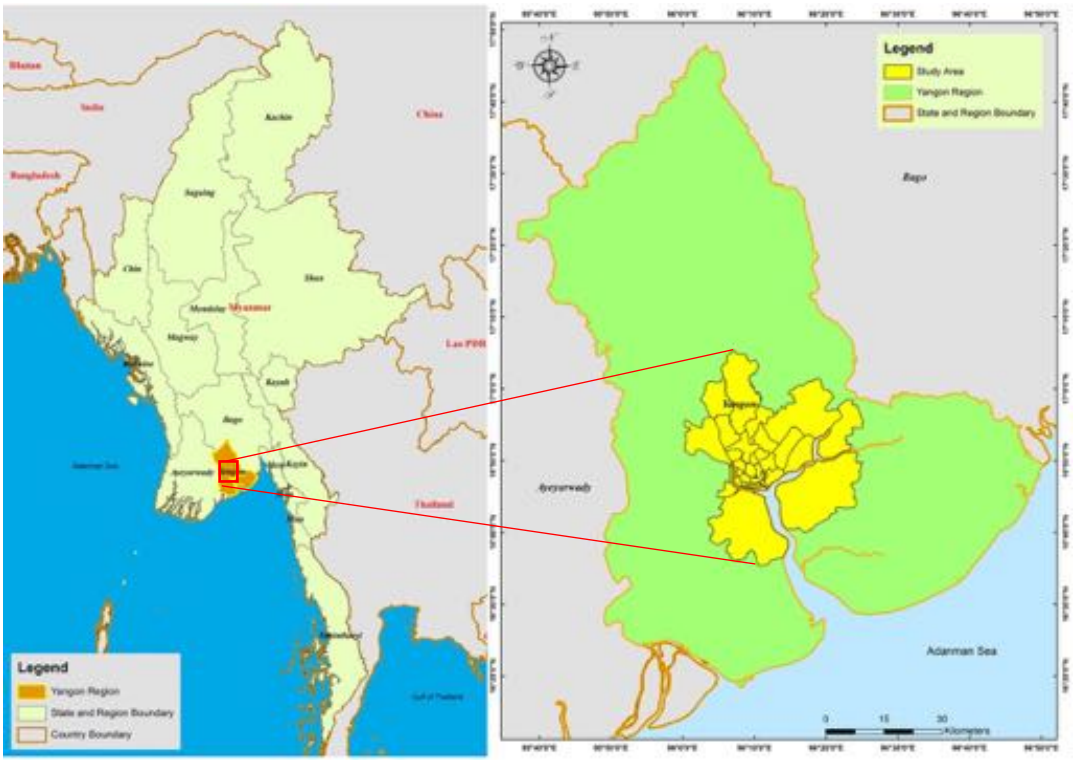

Figure 1.1. Location of the Study Area

the national population growth rate was 0.9% [2]. Due to the rapid population growth rate, the urban infrastructure in Yangon is deteriorating, and the government is concerned about how to solve that problem. Thus, we selected Yangon as a study area for our research.

1.3 Problem Statement

Yangon, the former capital and the most densely populous city in Myanmar, has occurred many problems in a number of areas, including massive expansion of building construction, traffic jams, solid waste management, and flooding. As the land consumption and urban changes are expanding, the government officials are facing many obstacles, and the timely and accurate land cover map and detection of changes are very important in solving these obstacles. The government does not have enough ground survey data as there has been no attempt to map and investigate changes in the past few years. For this reason, this study uses Landsat satellite's 30 years data to obtain valuable and reliable land cover information that is very useful for urban planning.

Landsat images with a resolution of 30m are free for research purposes, and many types of research related to the land cover classification of Landsat images have been developed over past forty years. Land cover classification using pixel-based approach has limitations such as mixed-pixels and salt-and-pepper effects. This means that the images have noise due to the low resolution of images like Landsat [3]. Moreover, remote sensing community has challenges in integrating multiple temporal, spectral, spatial and angular feature selection from remote sensing data, and the contribution of different features to land cover classification's accuracy remains uncertain [4].

1.4 Research Objectives

To solve the above-mentioned problem, the primary aim of this study is to perform land cover classification using time series satellite data and to identify change detection of land cover for the study area. The main objectives of this study are summarized as follows:

- To achieve accurate and effective land cover map that can be used in future urban planning by performing features level fusion using open social data and GIS metadata.
- To perform faster classification process using highly interactive machine learning algorithms with the cloud-based Google Earth Engine (GEE) platform.
- To evaluate which GEE machine learning algorithms provides the best land cover classification accuracy.
- To solve the salt-and-pepper effect, the features extracted based on the pixel-based approach are combined with the features extracted based on the object-based approach.
- To determine the trend of land cover changes for the study area in the periods from 1987 to 2017 using post-classification method.

1.5 System Overview

In our proposed system, the classification of land cover in the study area is performed by using GEE machine learning models and the changes over 30 years is analysed based on the post-classification comparison approach. The satellite images over 5 years from 1987 to 2017 are collected, and the image pre-processing for acquired images are performed as the first step in GEE as shown in Figure 1.2. After performing pre-processing stage, some additional spectral indexes such as Normalized Difference Vegetation Index (NDVI), Normalized Difference Build-up Index (NDBI), and slope values from SRTM 30m are combined with the input images before running into the machine learning classifier.

To train the dataset with a classifier, features from the Landsat image are extracted using pixel-based and colour composite approaches, and another features from Sentinel 2 image are extracted using object-based segmentation approach. In

addition, features from Open Street Map (OSM) and GPS metadata are also integrated into the 2017 data set. The data set is trained in machine learning model. The obtained classified map is evaluated through the accuracy assessment. Then change detection is investigated by using post-classification and land cover change maps are achieved at the final stage.

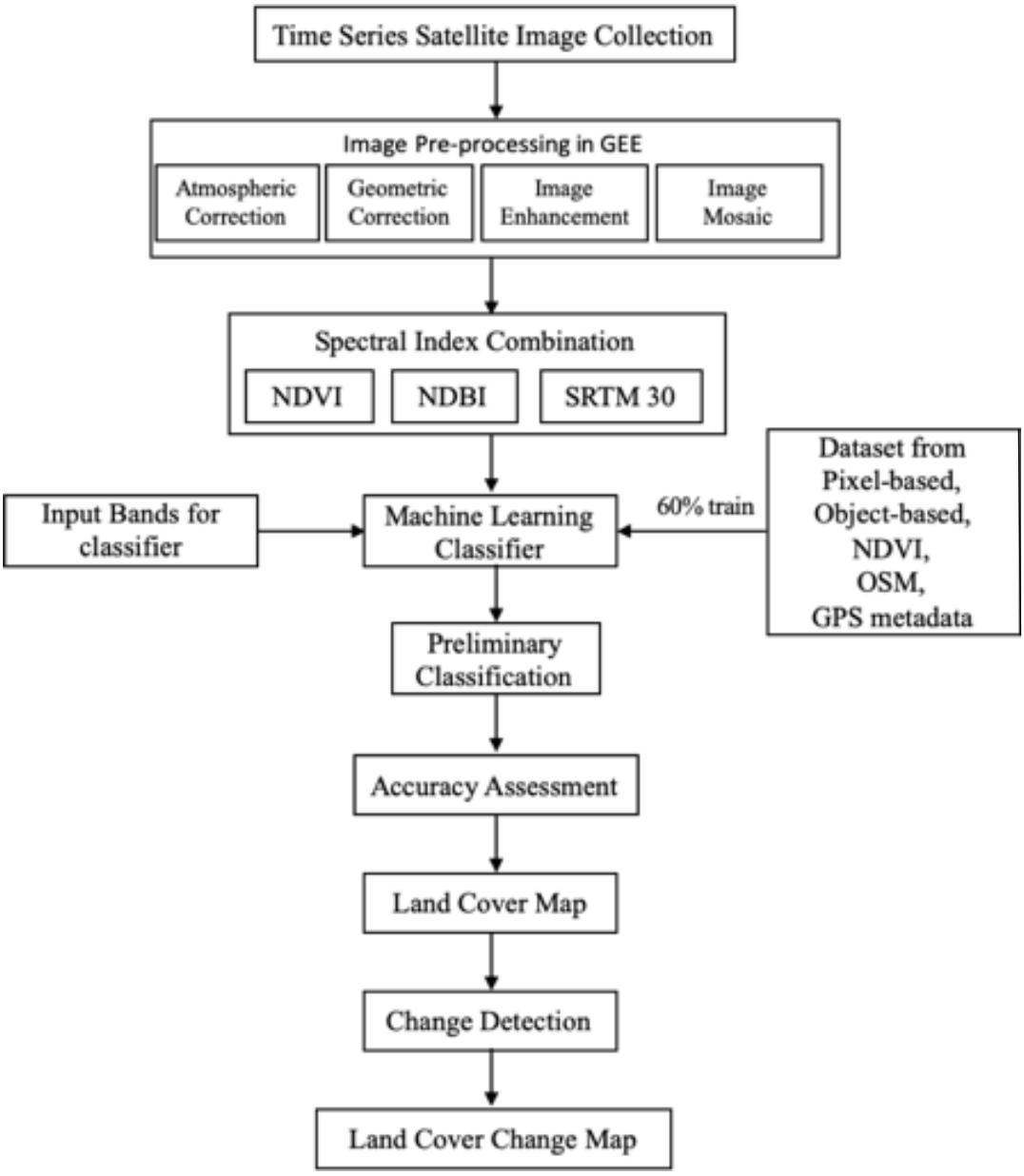

Figure 1.2. General Overview of the Proposed Method

1.6 Organization of the Research

The thesis study is organized as follows. Chapter 1 primarily introduces the background of the study. And then, the nature of the study area, problem statement, objectives, system overview and the organization of the research is explained. A literature review of land cover, remote sensing, time series data, machine learning, and their related researches are discussed in Chapter 2. This chapter briefly explains how remote sensing applications are utilized in land cover change detection study.

Chapter 3 describes the methodology and the materials used in detail, such as data collection, image pre-processing and spectral index combination. Then the different types of image classification are described. The theoretical background of machine learning classifiers and the accuracy is concisely explained. Detailed implementation and analysis of the experiment are provided in Chapter 4 with a discussion of the results. Chapter 5 concludes the research works and recommends future study.

CHAPTER 2
LITERATURE REVIEW

2.1 Land Cover and Land Cover Change

Land cover, which is a fundamental variable that affects human and physical environments, represents the physical conditions of the surface in the form of natural features such as soil, forests, agriculture, river, cropland, bare land, etc. Initially, the concept of land cover originated from the type and condition of vegetation of the area. However, it was later expanded to consider artificial structures in continuous utilization such as bridges, buildings, and roads, as well as the characteristics of the natural environments such as biodiversity, surface and ground-water, soil types [5]. Land cover data is available in raster and vector formats where individual land cover types are assigned to discrete value of the class. The use of land cover data and maps in urban planning can help better understanding of the impacts of natural phenomena and human use of the landscape.

The land cover change, also called land change, is a generic term for the human modification of the earth's surface [6]. There are commonly two main categories in land cover change namely conversion (a change of land cover class to another e.g. from forest to shrub land) and modification (a change within one land cover category e.g. from rainfed cultivated area to irrigated cultivated area) [7]. Nowadays, analysing of land cover change on a global scale is an important topic among land remote sensing communities because inadequate management of land resources leads to serious environmental problems.

Although many experiments using different approaches have been developed in the last thirty years, remote sensing and geographic information system (GIS) techniques are acquiesced as the powerful tools and are extensively applied for the investigation of spatiotemporal dynamics of land cover change [8,9]. Modelling land cover change using satellite image is one of the leading and effective ways to determine the current human footprint from the planet.

Land cover change can be detected based on the availability of regional and global land cover products supported in a wide variety of options. Different satellite sensors provide different resolution images that can be investigated for our own

related research. Some high-resolution satellite images cannot be freely accessed for the research purpose. In the previous few years, some investigations for land cover are focused on the utilization of deep learning model in high-resolution images. Technology is evolving every day and land cover change detection can be made more accurate and effective by using those techniques and models.

2.2 Remote Sensing

Remote sensing is the science and the art of obtaining information about an object, area, or phenomenon through the analysis of data acquired by devices that are not in direct contact with the object, area, or phenomenon being studied [10]. Canada Centre for Remote Sensing (CCRS) [11] defines remote sensing as the science of acquiring information about the surface of the earth without actually touching it. This is done by sensing and recording the reflected or emitted energy and processing, analysing, and applying that information. Remote sensing system consists of seven stages and the process of each stage is shown in Figure 2.1 [11].

According to Figure 2.1, the primary requirements for remote sensing are the electromagnetic radiation and electromagnetic spectrum. Frequency and wavelength are the two characteristics of electromagnetic radiation that are necessary for the understanding of remote sensing especially for the extraction of the information. The electromagnetic spectrum is described by the ranges from shorter wavelengths to longer wavelengths. Gamma and X-rays are types of the shorter wavelengths and microwaves and broadcast radio waves have longer wavelengths than others [11].

Remote sensing is performed using a sensor instrument and the modern Earth remote sensing began in 1972 when the National Aeronautics and Space Administration (NASA) provided the Landsat Multispectral Scanner System (MSS). Remote sensing images are acquired passively (e.g. digital camera) or actively (e.g. RADAR, LiDAR) from sensors. Reflected and emitted wavelengths from the Earth's surface are measured naturally by passive remote sensing. However, in active remote sensing, sensors from third parties of satellite equipment emits energy to the target area and the reflected radiation of the specific area is detected [11].

The term *resolution* is commonly used to describe remote sensing images and there are four different types of resolution: spatial, spectral, radiometric, and temporal resolution. Spatial resolution, the pixel size, is the assignment of the smallest angular or linear spacing between two objects performed by a remote

sensing system. Spectral resolution is the ability of the sensor to identify the narrow dimension of the wavelength intervals of a particular band in the electromagnetic spectrum. The quantization level, which is the actual number of signals in a band of the image is specified as the radiometric resolution. The concept of temporal resolution is also important for remote sensing system, which refers to the sensor's revisiting time to acquire an image of a particular area [11,12].

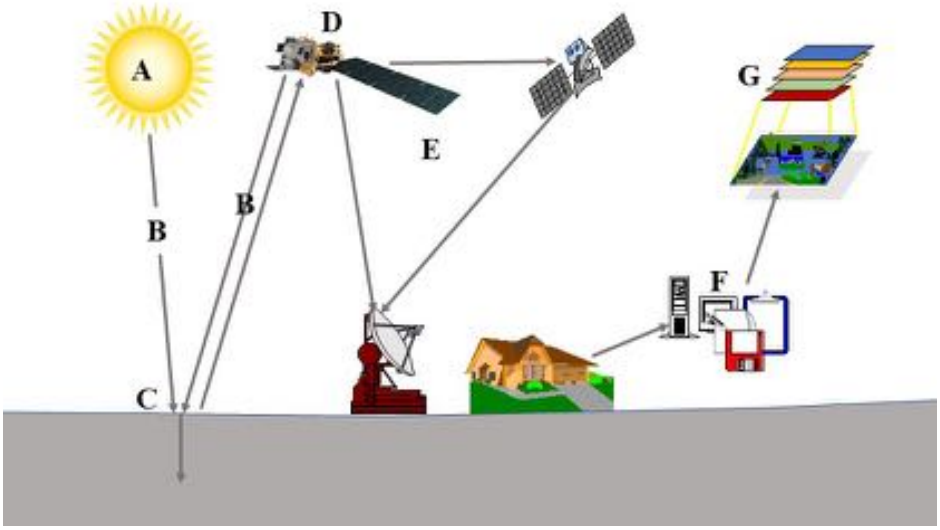

A: Energy Source or Illumination

B: Radiation and the Atmosphere

C: Interaction with the Target

D: Recording of Energy by the Sensor

E: Transmission, Reception, and Processing

F: Interpretation and Analysis

G: Application

Figure 2.1. System of Remote Sensing

2.3 Machine Learning

Remote sensing data cannot be applied directly to related fields and computer algorithms such as machine learning and deep learning are necessary to obtain information that are useful for experts and decision makers. In this research, machine learning algorithms are implemented for the land cover classification in the study area. Machine learning is the part of artificial intelligence and the computational

methods. These methods can improve program performance by learning from the data and past experiences. Machine learning provides knowledge to computers from data set and observations of the human's experiences [13].

Even though machine learning consists of different types of algorithms based on their learning style and function, all algorithms consist of with three steps: representation, evaluation, and optimization [13]. Learning techniques in machine learning depend on the patterns of the data used, the statistic, and the concept of data analysis in computer science. There are different approaches to learn for machines such as supervised learning, unsupervised learning, semi-supervised learning, reinforcement learning, active learning, transduction inference, and so on. Among the different learnings, four major approaches are discussed in our research.

2.3.1 Supervised Learning

A machine learning model that can perform prediction on new data by learning an input training dataset that includes inputs and labels is called supervised learning. In a supervised model, the correct output is known based on the evidence of present uncertainty, and the algorithm iteratively investigates predictions on the training data. Learning is stopped when the algorithm reaches to an efficient level of performance.

Supervised learning is faster and more accurate than the other learning and can be grouped into classification and regression. Classification is the process of determining or predicting the output of a model into different categories based on the input training classes (for example, an email is spam or not, the picture is fake or real, etc). Regression is used to predict continuous response values (for example house prices, changes in water levels, population of the cities, etc) [14,17]. Popular types of supervised algorithms include linear regression, random forest, support vector machine, decision tree, Naive Bayes, nearest neighbour, and so on [15].

2.3.2 Unsupervised Learning

Unsupervised learning uses unlabelled data sets to train models in a computer and the system has to find hidden patterns from the given data. The training dataset in unsupervised learning has no structure that includes noisy data, mixed data, and unknown data, and so on. It is very useful when data scientists do not know what

type of class or pattern is being learned from the data. Examples of unsupervised learning problems are clustering, and dimension detection, which group similar features. Common unsupervised algorithms include k-means clustering and association rules [15-17].

2.3.3 Semi-supervised Learning

Semi-supervised learning is a model includes a large amount of training data, which are both labelled and unlabelled, and predicts unseen data based on the mixture of supervised and unsupervised. Since label data is expensive and time-consuming, most real-world problems are investigated by semi-supervised learning. Furthermore, the collection of unlabelled data is easy and performed in a short period. Application with various types of problems including classification, regression, or ranking tests can be assumed as the instances of semi-supervised learning [14,16].

2.3.4 Reinforcement Learning

The training and testing phases are performed together in reinforcement learning and decisions are made based on active learning of the environment. Based on the training of the input data, the model interacts with the environment and returns states based on the cases that occurred in the environment. The best model can be determined based on the maximum reward that the user assigns to the output. There are two types of reinforcement learning: positive reinforcement that has a positive effect on the behaviour and negative reinforcement strengthens the behaviour by avoiding negative conditions [14,18].

2.4 Change Detection

The process of investigating differences in the state of object or circumstance by analysing it over a period of time is called change detection [19]. Thus, at least two or more time series conditions are required to perform change detection. Due to the development of numerous data acquisition from satellites, many data scientists and environmental researchers have been interested in the area of change detection research using remote sensing. Better management of natural resources depends mainly on timely and accurate change detection of the earth's surface that support the phenomenon and relationship between human beings and their environment [20].

Therefore, land cover change detection has become into one of the popular topics in the research area of the remote sensing communities.

Meticulous change detection data can be used in many diverse applications such as urban planning, disaster assessments, deforestation analysis, land use change analysis, investigation of snow-melt, crop mapping, seasonal change in pasture production, and other environmental monitoring processes [19]. To achieve better change detection, area change and change rate, the spatial distribution of changed types, change trajectories of land cover types, and accuracy assessment are indispensable [20].

Image overlay, image algebra, post classification comparison (PCC), change vector analysis, principal component analysis, and change vector analysis are widely used methods in the land cover change detection. PCC, the delta classification, is the most popular approach among them. In PCC, land cover classification is first performed on the label classes and the area of change is calculated using a direct comparison of the same spectral information class [12,20].

2.5 Related Works

Several studies have been done for land cover classification and change detection using Landsat data in the last 30 years. However, classification accuracy and effective analysis of changes still have limitations due to image resolution, computation time, ground truth data availability, machine learning performance, and deep learning models. Land cover classification is performed using wide varieties of approaches, including pixel-based, object-based, combination of pixel and object-based, sensor fusion, feature fusion, and others to achieve accurate and useful results.

R. Jhonnerie et al. [21] evaluated mangrove land cover mapping using Landsat 5 and ALOS PALSAR imageries in Kembung River, Bengkalis Island, Indonesia. The results achieved by the random forest classifier using object-based image analysis (OBIA) were compared with other results of common pixel-based classifier (e.g. maximum likelihood). NDVI, NDBI, and normalized difference water index (NDWI) were also examined by both classifiers.

After Google.org introduced GEE in 2010, many scientists especially earth scientists and conservationists start to focus on the utilization of GEE for its computational performance and open data access. Y. H. Tsai et al. [22] implemented

a GEE based image classification method that can classify forest cover and land use types while minimizing cloud and terrain issues. The optimal parameters for machine learning model are evaluated based on tuning methods. Multi-temporal spectral vegetation index (SVI) composite is considered for higher accuracy results.

U. Pimple et al. [23] proposed a new strategy to implement pre-defined knowledge-based rules to obtain error-free 30-year annual composites of Landsat data for mangrove mapping in the Trat Province of Thailand and the land use land cover (LULC) of the surrounding on the GEE. Their strategy achieved the outstanding overall accuracy of 0.96 followed by a kappa coefficient 0.94 in 30 years of classification results.

Some researches focus on time series data of satellite images in combination with geographic information system (GIS). G. T. Ayele et al. [24] employed Bayesian classifier based land cover mapping based on training data extracted by GIS to estimate the probability for each land cover category using mean and variance values. The 12 major land cover classes for Northern Ethiopia was classified in 20 years and the spatiotemporal dynamic changes were calculated using post-classification and statistical approach.

Land cover change detection in large area like global or continental skill takes time-consuming and requires a high-speed supercomputer. GEE can solve those kinds of difficulties. A. Midekisa et al. [25] applied GEE platform to quantify land cover and impervious surface change for 15 years on Africa continent using Landsat satellite image collection. Night-time light data was also used for Random Forest (RF) classification and output classification was compared to the Hansen product.

Satellite data is taken all year around and those data can be regarded as big data because of their large image collection and data storage capacity. Exploration of GEE platform for big data processing as described in A. Shelestov et al. [26] and multi-temporal satellite image from multiple sensors are used for their research. Country level crop mapping was experimented using different machine learning classifiers of GEE. They discussed the advantages and disadvantages of those classifiers.

J. Xiong et al. [27] used Landsat 8 and Sentinel 2 data on GEE to highlight the methodology for mapping of cropland area across the Africa continent by using Landsat 8 and Sentinel 2 data on GEE. Temporal synthesis of two sensors was

performed for two crop growth periods with an 11 band stack and two pixel-based supervised methods: RF and support vector machine (SVM) were executed for the classification.

T. Sritarapipat et al. [28] has predicted urban expansion in Yangon based on the multi-centres of the urban area and the class translation matrix obtained from land cover classifications. They developed an urban growth model derived from a dynamic statistical approach using Landsat data from 1978 to 2009 and Stereo GeoEye data in 2013.

Y. Wang et al. [29] analysed changes of land cover patterns and their influences on surface temperature change in Yangon, Myanmar. Land cover change detection from 1987 to 2015 was characterized from the Landsat satellite, and surface temperature was derived from the MODIS satellite. This study also describes two major differences from previous experiments on the impacts of land cover on surface temperature.

The use of a cloud-based GEE platform in combination with GIS and other remote sensing methodologies is very effective and efficient for researche and the environmental community. The advantages of GEE and remote sensing can be seen in the above experiments. Furthermore, proper use and selection of machine learning models based on requirements are important to achieve excellent output. Therefore, we perform land cover classification based on pixel and object-based approaches using GEE time series data and also calculate spectral index to obtain reliable results.

CHAPTER 3
MATERIALS AND PROPOSED METHOD

3.1 Data Used

The chapter of data collection provides brief description of the materials used in this study, especially satellite data set. The training data set includes satellite images, open social data and GPS metadata. Although this study focuses on time series data set, Sentinel 2, open social data, and GPS data can only be obtained in the recent years. Thus, Landsat 5, Landsat 7, Landsat 8 image collections are executed from 1987 to 2012.

3.1.1 Landsat 5

The Landsat program is the oldest and longest earth observatory digital satellite imaging system. NASA and US Geological Survey (USGS) lunched Landsat 5 on March 1, 1984 and equipped with two sensors: the MSS and the Thematic Mapper (TM). Although the Landsat MSS has a spatial resolution of 57m and contains four spectral bands, the TM sensor was designed to improve geometric and radiometric accuracies, as well as spatial and spectral resolutions as compared to the MSS sensor. Mid-infrared band and the thermal band are added to Landsat TM sensor to achieve better spectral resolution. There are seven spectral bands in TM. The TM also has a ground sampling interval of 30m reflection and 120m thermal value [30]. Table 3.1 and 3.2 shows the characteristics of Landsat MSS and TM.

Table 3.1 Characteristics of Landsat MSS

Band	Description	Spectral Resolution (μm)	Spatial Resolution (m)
MSS1	Green	0.5 – 0.6	57
MSS2	Red	0.6 – 0.7	57
MSS3	Near-Infrared (NIR) 1	0.7 – 0.8	57
MSS4	Near-Infrared (NIR) 2	0.8 – 1.1	57

Table 3.2 Characteristics of Landsat TM

Band	Description	Spectral Resolution (μm)	Spatial Resolution (m)
B1	Blue	0.45 – 0.52	30
B2	Green	0.52 – 0.60	30
B3	Red	0.63 – 0.69	30
B4	Near-Infrared (NIR) 1	0.76 – 0.90	30
B5	Near-Infrared (NIR) 2	1.55 – 1.75	30
B6	Thermal	10.4 – 12.5	30
B7	Mid-Infrared	2.08 – 2.35	30

3.1.2 Landsat 7

The Landsat 7 was launched from Vandenberg Air Force Base in California on April 15, 1999. It was operated by National Oceanic and Atmospheric Administration (NOAA), NASA, and USGS. It was placed on the Delta II rocket and carried an earth observing sensor called Enhanced Thematic Mapper (ETM^+). It has higher capabilities than TM instruments on Landsat 4 and 5 because it includes additional features like 15m spatial resolution of panchromatic band, 5% radiometric calibration, 60m resolution of thermal IR channel and onboard data recorder. Thus,

Table 3.3 Characteristics of Landsat ETM^+

Band	Description	Spectral Resolution (μm)	Spatial Resolution (m)
B1	Blue	0.45 – 0.52	30
B2	Green	0.52 – 0.60	30
B3	Red	0.63 – 0.69	30
B4	Near Infrared (NIR)1	0.77 – 0.90	30
B5	Near Infrared (NIR) 2	1.55 – 1.75	30
B6	Thermal	10.4 – 12.5	30
B7	Mid-Infrared	2.08 – 2.35	30
B8	Panchromatic	0.52 – 0.90	15

Landsat 7 has 8 bands, as shown in Table 3.3 and is considered as the most accurately calibrated earth observation satellite. It will be replaced by Landsat 9 in late 2020 [31,32].

3.1.3 Landsat 8

The Landsat 8 includes two sensors called Operational Land Imager (OLI) and Thermal Infrared Sensor (TIRS). The characteristics are shown in Table 3.4 including their spectral and spatial resolution values. It was launched on Feb 11, 2013 from Vandenberg Air Force Base, California on an Atlas-V rocket. The OLI sensor was built in 9 bands (B1 to B9) by Bali Aerospace & Technologies Corporation and TIRS was built with 2 bands (TIRS1 and TIRS) by NASA Goddard Space Flight Centre [33,34].

Table 3.4 Characteristics of Landsat OLI and TIRS

Band	Description	Spectral Resolution (μm)	Spatial Resolution (m)
B1	Ultra-Blue	0.435 – 0.451	30
B2	Blue	0.452 – 0.512	30
B3	Green	0.533 – 0.590	30
B4	Red	0.636 – 0.673	30
B5	Near Infrared (NIR)	0.851 – 0.879	30
B6	Shortwave Infrared (SWIR) 1	1.566 – 1.651	30
B7	Shortwave Infrared (SWIR) 2	2.107 – 2.294	30
B8	Panchromatic	0.503 – 0.676	15
B9	Cirrus	1.363 – 1.384	30
B10	Thermal Infrared (TIRS) 1	10.60 – 11.19	100 * (30)
B11	Thermal Infrared (TIRS) 2	11.50 – 12.51	100 * (30)

Since TIRS sensor has a spatial resolution of 100m, the fundamental purpose is to collect surface temperature characteristics and to investigate the process of heat and moisture transfer in the related environments. Ultra-Blue band in OLI is also essential for the coastal and aerosol studies. The approximate scene size for Landsat

8 is 170km north-south and 183km east-west and its data are taken on the Worldwide Reference System-2 (WRS-2) path system [33].

3.1.4 Sentinel 2

Copernicus Sentinel 2 was launched as part of the European Commission's Copernicus program on Jun 23, 2015. The main objective is to support land monitoring and management. It was built with two polar orbiting satellites and carries Multispectral Instrument (MSI) in 13 spectral bands. The detailed characteristics are described in Table 3.5. The coverage area of Sentinel 2 is from between latitudes 56° south and 84° north with 7-year of design life [35].

Table 3.5 Characteristics of Sentinel 2

Band	Description	Spectral Resolution (μm)	Spatial Resolution (m)
B1	Coastal aerosol	0.433 – 0.453	60
B2	Blue	0.458 – 0.523	10
B3	Green	0.543 – 0.578	10
B4	Red	0.650 – 0.680	10
B5	Red-edge 1	0.698 – 0.713	20
B6	Red-edge 2	0.733 – 0.748	20
B7	Red-edge	0.773 – 0.793	20
B8	Near Infrared (NIR)	0.785 – 0.900	10
B8A	Near Infrared narrow (NIRN)	0.855 – 0.875	20
B9	Water vapor	0.935 – 0.955	60
B10	Cirrus	1.360 – 1.390	60
B11	Shortwave Infrared (SWIR) 1	1.565 – 1.655	20
B12	Shortwave Infrared (SWIR) 2	2.100 – 2.280	20

3.1.5 Open Street Map

Open Street Map (OSM) is a voluntary geographic information project under the Open Database License (ODbL) and provides open data that freely available from all perspectives under the license agreement. It is an international not-for-profit

organization and is a worldwide mapping effort with more than one million contributors worldwide. It supports geospatial information about roads, buildings, streets, bridges, stations, rivers, and others based on aerial imagery, GPS devices, and low-tech field maps. Users can access OSM data in vector format including with point, line and polygon geometries [36].

3.1.6 GPS Metadata

Global Positioning System (GPS), a satellite-based navigation system, is used to track information from GPS satellite and then calculate the geographical position of the device. The GPS device can be used worldwide with associated software, as the U.S. government allowed to access data freely for civilian purposes. GPS is widely used in many fields, and the land cover field is used to collect the ground-truth coordinates of the land cover class. A GPS device receives the radio signals transmitted from the satellite and technicians transform those units into the metadata in terms of latitude, longitude, and altitude to determine the location of the ground [37].

3.2 Image Pre-processing

Image pre-processing is an important step in satellite image processing procedure. Since satellite images are taken from locations very far from the surface of the earth, they have many noises, distortion, and errors during scanning, transmission, and recording of the data. Typically, pre-processing includes denoising, radiometric correction, geometric correction, image sub-setting, image mosaicking, and image enhancement. At least one or more operations need to perform as pre-processing to obtain useful information from the images [10]. In this study, we manipulate atmospheric correction, geometric correction, image mosaicking, and image enhancement for images used in land cover classification.

3.2.1 Radiometric Correction

The process of compensating for atmospheric effects to improve the accuracy of surface spectral reflectance, emittance, or back-scattered measurements obtained from the satellite sensors is called radiometric correction. When satellite images are directly analysed without correction, the illuminations, scattering,

refraction, clouds, haze, and other particles in the atmosphere will affect the quality of the image [12]. Furthermore, the images used in this study are acquired from the Landsat and Sentinel 2, and those images are taken from 10 to 30 m above ground level. Therefore, it is necessary to perform radiometric correction on the input image collections.

There are many methods of radiometric correction depending onto the atmospheric radiation matters and applied environments. Among them, the atmospheric correction method is applied in our approach because we extract land cover information from the satellite image and then compare and detect changes. Sometimes atmospheric effects can be ignored when a single date of remotely sensed data is used in the classification. Atmospheric correction is executed in GEE using cloud removal algorithm on Landsat and Sentinel 2 data.

3.2.2 Geometric Correction

Geometric correction is known as the process of assigning the reflected, emitted and back-scattered measurements of electromagnetic radiation in the proper planimetric location by using applied geographic reference system [12]. Since satellite images contain a very wide area, we have to select an appropriate projection for that study area. Most of the scientists often applied two common geometric correction methods: image-to-map rectification and image-to-image registration. In our study, datasets are assigned to the UTM WGS 84 system using image-to-image registration as part of pre-processing.

3.2.3 Image Mosaicking

Image mosaicking is a combination of multiple images from satellite to achieve a single seamless composite image for the study area [12]. The satellites collect images based on their orbital paths, and a coverage of the study area may exist between two or more images. Thus, we have to perform mosaicking in our study. In addition, layer stacking that combines multiple separate bands or layers into one single image is also essential in the pre-processing sequence of our approach because image fusion is executed from Landsat 8 and Sentinel 2 satellites. These image mosaicking and layer stacking are implemented in GEE before enhancing the images.

3.2.4 Image Enhancement

The major purpose of image enhancement is to improve the visual interpretability of an image by upgrading the image definition, and contrast and emphasizing the necessary attributes in the image. The selection of the digital image enhancement approach depends upon the extracted features to be used from the image. Contrast manipulation, spatial feature manipulation, and multi-image manipulation are the most commonly used enhancement approaches. The remotely sensed image has a parameter called spatial frequency. The frequency can be enhanced by using spatial convolution filtering and Fourier analysis [10,12]. In this research, median filtering (one filtering type of spatial convolution) is executed in GEE to reduce noises in the image.

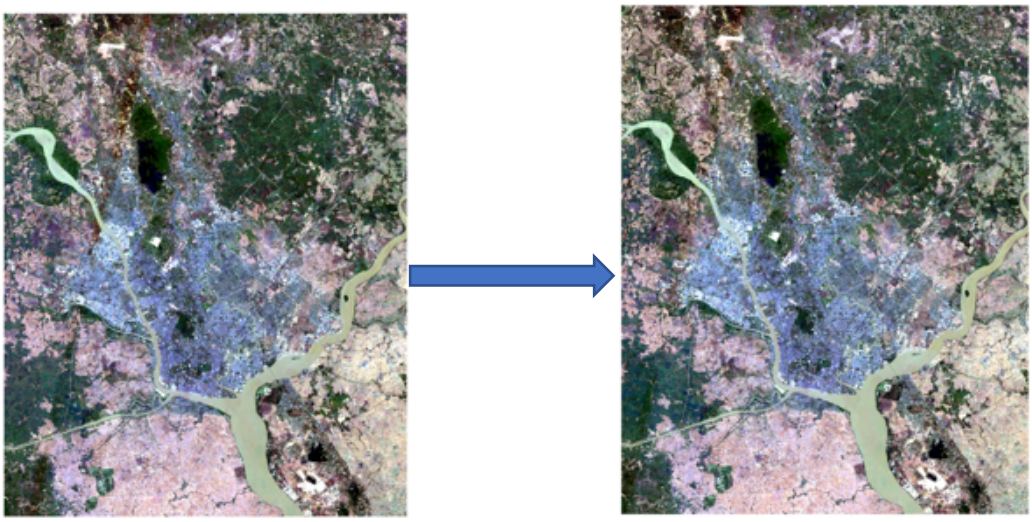

Figure 3.1. Before and After image pre-processing of True Colour Landsat Image

Figure 3.1 demonstrates the before and after applying image pre-processing approaches in Landsat 8 true colour image. The analysis of histogram for the spectral bands of satellite images can indicate the nature of the image. The histogram analysis of Landsat image before and after image pre-processing is obtained as shown in Figure 3.2 and 3.3 respectively. The significant change occurs in B1 of Landsat image because this band is especially used for the studying of coastal and aerosol. The aerosol is one of the important features in studying atmospheric monitoring. When our approach removes the cloud from the image, the spectral value of B1 is decreased.

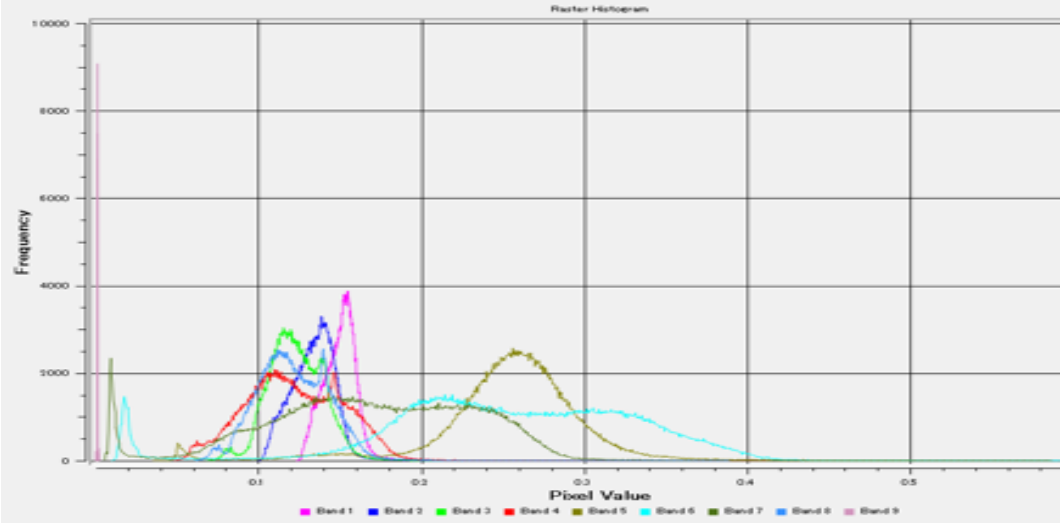

Figure 3.2. Spectral band histogram analysis of raw Landsat image before image pre-processing

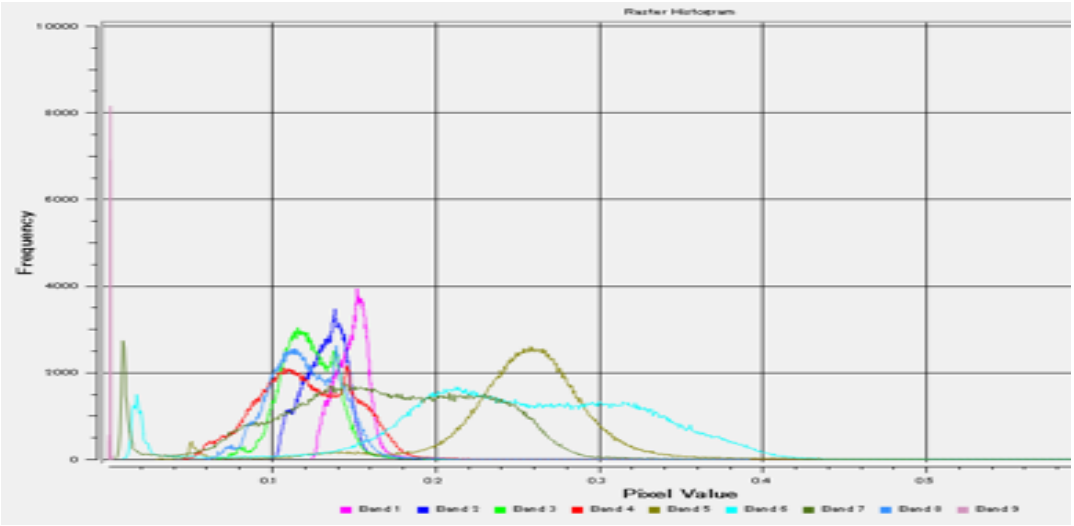

Figure 3.3. Spectral band histogram analysis of raw Landsat image after image pre-processing

3.3 Spectral Indices and Layer Combination

Spectral indices are a combination of two or more spectral wavelengths. They are used to emphasize specific features or phenomena in the processing of remotely sensed images. There are many different types of spectral indices that can be used in scientific applications. Capabilities of spectral indices become crucial in the exploration and evaluation of the land cover classes. In our classification approach, we first calculate NDVI and NDBI values. Then slope value is extracted

from the SRTM. After that, those two spectral indices and slope value are added to the input image. The processed image is used in the classification as a band combination process to achieve high classification accuracy. Since the study area is a modernized city, we only focus on to calculate NDVI value to detect changes in vegetation, agriculture and the NDBI value to detect changes of building.

3.3.1 Normalized Difference Vegetation Index (NDVI)

Approximately 70% of the earth's surface is covered with vegetation. Thus, understanding the spectral features related with vegetation species is essential to remote sensing community. The NDVI is the most common index used in the study of vegetation. It can be calculated by measuring the differences between near-infrared (NIR) and the red band as the following equation.

$$NDVI = \frac{NIR-RED}{NIR+RED} \quad (1)$$

Where NDVI stands for normalized difference vegetation index, NIR is the near-infrared band, and RED is the red band of the associated satellite's sensors. The range of NDVI is between -1 to 1. NDVI is widely used to detect changes vegetation reflectance especially for the forest, agriculture, and crop types. When NDVI value is negative, that area is likely water as the reflection of water in the red is higher than the NIR. NDVI value close to +1 can be regarded as the dense forest with green leaves. With the NASA statement, NDVI can also be used as a good indicator of drought [12,38].

3.3.2 Normalized Difference Build-up Index (NDBI)

Many scientists and professionals who are working in urban planning sectors focus on the research and monitoring of the urban spatial distribution and differentiation. The normalized difference build-up index (NDBI) is the most common index used for the mapping of urban and build-up areas. Today, the urbanization is increasing around the world and the NDBI is one of the important spectral indices in satellite image processing. The NDBI can be calculated according to equation (2):

$$NDBI = \frac{SWIR-NIR}{SWIR+NIR} \quad (2)$$

Where NDBI means normalized difference build-up index, SWIR is the shortwave infrared band, and the NIR is near-infrared band of the associated satellite's sensors [12].

3.3.3 SRTM

The shuttle radar topography mission (SRTM) provides the most complete highest-resolution digital elevation data of the earth at the global scale for researchers. The SRTM was lunched abroad in the space shuttle Endeavor on Feb 2000 by a joint project of NASA, the National Geospatial-Intelligence Agency, and the German and Italian Space Agencies. Since extra features related to the Earth's surface are considered in land cover classification, the performance of classifier models can be increased. Thus, slope value extracted from SRTM 30-m dataset is added as an extra feature in our classification process [39].

3.4 Feature Extraction of Satellite Imagery

Feature extraction of satellite image can be regarded as process of collecting data to train in machine learning classifiers. Feature extraction methods will vary depending on the expected classification results. Myanmar is a developing country and the government lacks accurate and useful datasets that are acquired by surveying methods. Thus, we extract features for training dataset from satellite images using GIS techniques. In GIS, vector data exists in the form of point, line, and polygon, and all forms have their associated features. In our experiment, we collect land cover training data in polygon form using pixel-based and object-based approach.

3.4.1 Pixel-based Approach

The cells of a raster are extracted as a polygon based on the spatial and spectral values in pixel-based approach. The spatial values are pixel size and pixel scale of image and the spectral values consists of wavelength ranges. There are numerous methods to extract image pixels. Among them, our approach conducts

features extraction using colour compositing of multispectral satellite images. Collection of sample data using colour composite is performed in ArcGIS. When multispectral image visualization is performed, it is possible to use a single band or combination with other bands at a time. In satellite images, there are more than 3 bands and we can composite those bands for visual display.

Red, green and blue are primary colours of image and combination of these three colours with other bands produces colour composite image. True-colour image is a combination of 3 primary bands wavelength ranges of the visible spectrum. It is approximately same as the image that can see by human eyes.

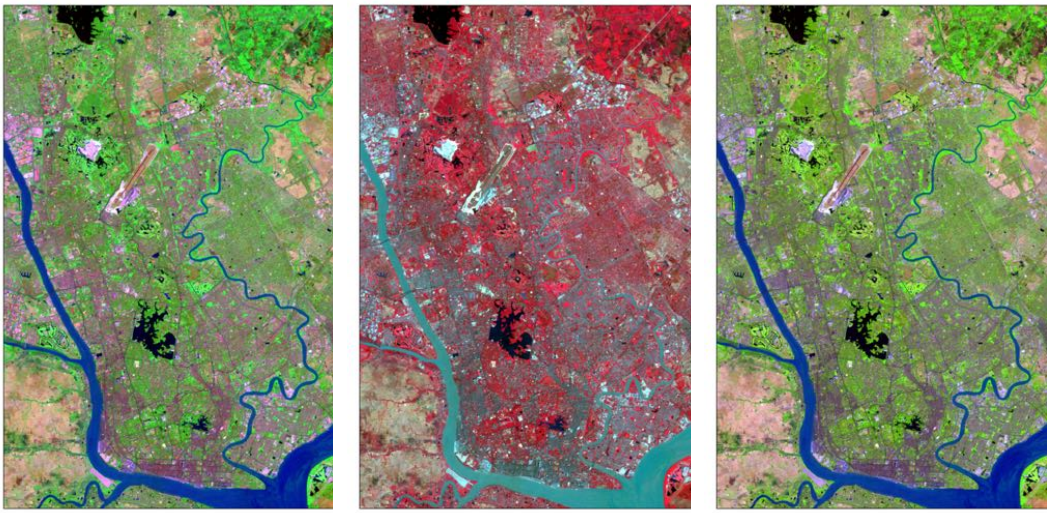

(a) (b) (c)

Figure 3.4. False Color Composite of Landsat OLI Image

Multispectral images that contain any other combinations of bands outside the visual bands is regarded as the false-colour image [12]. Different land cover classes can be extracted based on the composite approaches.

When green, NIR, and SWIR 2 bands are combined, the output false-colour image is resulted as shown in Figure 3.4(a) and water body and bare soil are extracted using this false colour composite. Shrub land and vegetation are collected from false-colour image that is a combination of red, green, and NIR band as shown in Figure 3.4(b). Combination of red, NIR and SWIR 1 band produces false-colour composite that is shown in Figure 3.4(c) and urban area and forest are extracted from that composite.

3.4.2 Object-based Approach

In object-based approach, features are extracted by segmenting images into image objects with similar spectral, spatial, and texture characteristics. Segmentation of image consists of two key steps: (1) edge-based segmentation and (2) lambda schedule merging [40]. ENVI feature extraction is used in our study to perform object-based approach. It is a module to extract information from high-resolution panchromatic or multispectral imagery. As high-resolution image is necessary to perform segmentation, 10 m Sentinel 2 image is used in this approach.

The spatial, spectral, and texture features including 33 attributes are extracted using ENVI and workflow is designed with the combined process of segmenting image, creating the objects and classifying to extract features. First, a gradient map or intensity map is computed from image and choose scale level to delineate boundaries of objects. And then, Full Lambda-Schedule algorithm implemented by D. J. Robinson et al. [41] is implemented to perform merging. The adjacent segments are iteratively merged depend on the combination of spectral and spatial information until the algorithm exits. The merging algorithm will continue if the merging cost is less than a defined threshold lambda value evaluated from the following equation (3) and segment the modified map using a watershed transform.

$$t_{m,n} = \frac{\frac{|O_m|.|O_n|}{|O_m|+|O_n|}.\|u_m - u_n\|^2}{length(\partial(O_m, O_n))} \quad (3)$$

Where:

$t_{m,n}$ is the merging cost

O_m is region M of the image

O_n is region N of the image

$|O_m|$ is the area of region m

$|O_n|$ is the area of region n

u_m is the average value in region m

u_n is the average value in region n

$\| u_m - u_n \|$ is Euclidean distance between the spectral values of regions m and n

$length(\partial(O_m, O_n))$ is the length of the common boundary of O_m and O_n

3.5 Google Earth Engine

The google earth engine (GEE), a cloud-computing platform, enables scientific analysis and visualization of geospatial datasets using advanced machine learning algorithms. It supports free access to extensive catalogues of satellite images and other geospatial data. Those images and data can be used for the academic researches, non-profit and business organizations, and the government. Furthermore, it can be applied in pursuing a commercial application if the commercial license of earth engine is conducted. A variety of massive satellite images can be directly retrieved, and advanced image processing can be intensively tested and performed based on the machine learning algorithms on GEE [22, 26]. Since GEE operates with petabyte scale, it reduces processing times and optimizes the capacity in performing global scale analysis [25].

3.6 Machine Learning Classifiers in GEE

GEE offers several machine learning algorithms which can perform supervised and unsupervised classification. In this study, land cover classification of multispectral image is investigated using 6 different machine learning algorithms that achieve appropriate result for land cover, and their accuracies are compared. We briefly discuss GEE six machine learning algorithms which are applied in this research.

3.6.1 Random Forest

The RF is an ensemble classifier that combines a number of non-parametric classification and decision tree. It has been increasingly used in remote sensing fields especially for land cover classification because of the accuracy of their classifications. Classification and regression problems can be solved using RF and it can efficiently perform in handling of big data and enable to outlier and overfitting. Furthermore, RF is popular due to its determination of important variables and the ability to predict missing values [21,27]. RF model evaluates predictions using a forest of trees. Thus, a key to achieve successful model depends on how the forest is created using each of decision trees. So, number of trees and number of features in each tree become important parameter in implementing RF model [42,43].

3.6.2 Classification and Regression Tress

A decision tree-based model that performs classification based on historical data using the concept of information entropy is called classification and regression tree (CART). In CART model, binary decision trees are constructed from the learning of the training sample and decision is selected from the attribute with highest normalized information gain. Then, the right tree size is chosen to perform the model and classification of new data is executed based on the constructed tree. The CART also has non-parametric nature and can easily handle both numerical and categorical variables. Furthermore, it identifies most significant variable itself and eliminates a non-significant one. Even though it can easily handle outliers, it has high sensitivity to the training dataset [26,44].

3.6.3 Multiclass Perceptron

The simplest form of a neural network that is executed in classification problems is known as the perceptron. Basically, multiclass perceptron is regarded as the binary extension of linear perceptron to perform classification of two or more classes. Pattern classification is limited only for two classes if the perceptron is created around a single neuron. Thus, output layer must contain more than one neuron to work properly for multiclass classification. In multiclass perceptron model, a linear combination of the inputs applied to its synapses is added to the node of the neural network and output neuron's sum is applied to hard limiter. Hence, the neuron produces an output equal to -1 when hard limiter input is negative, and +1 if it is positive [45].

3.6.4 GMO Maximum Entropy

The GMO maximum entropy is a type of multinomial logistic regression models and is used to perform multiclass classification based on the linear regression generated from the SoftMax transformation of a linear function of the feature variables [46]. This model is constructed based on the maximum entropy principle which selects the model with greatest entropy depends on the approximate consistent with constraints [47]. The primary objective of model is to minimize an error function by selecting cross-entropy that is the negative logarithm of likelihood [45].

3.6.5 Minimum Distance

The minimum distance classifier is widely used in pattern recognition and also in remote sensing community because it is simple, robust and fast compared with other complicated classifiers. In the minimum distance model, the unknown patterns are classified into the classes based on the minimum measurement of similarities between distributed functions [48]. The minimum distance classification model is defined by using the following equation (4).

$$x \in w, if\ dist(x, zi) = \min\{dist(x, zj)\}, \forall j \quad (4)$$

Where x be an unknown pattern to be classified and zi (i = 1, ..., n) is a prototype for category ωi. x and z are m-dimensional vectors in the feature space, n is number of categories, and m is number of dimensions of the feature space. dist(·) is Euclidean distance function [49]

$$dist(x, zi) = \sqrt{\sum_{k=1}^{m}(xl - zik)^2}\ . \quad (5)$$

3.6.6 Continuous Naïve Bayes

Naïve Bayes is a simple but exceptionally powerful model which is based on the Bayes theorem stated in equation (6) and assumption of independence between input variables. Continuous Naive Bayes classifier is constructed to solve binary and multiclass classification problems. In this model, the target value is calculated based on the assumption of independent conditions rather than attempting to calculate the value for each attribute value. Due to the optimization procedures do not need to fit the coefficients, learning of Naïve Bayes model from training data is fast. Furthermore, it can reduce average risk of classification error in the learning procedure.

$$P(h|d) = \frac{P(d|h) \times P(h)}{P(d)} \quad (6)$$

Where P(h|d) be the posterior probability, P(d|h) be the probability of data d given that the hypothesis h was true, P(h) is the prior probability of h, and P(d) is the probability of the data [16,45].

3.7 Accuracy Assessment

When the classification of land cover using remote sensing data is finished, accuracy assessment of classifier model is necessary to determine performance of that model. There are various methods to assess accuracy of land cover classification. Among them, classification error matrix sometimes called a confusion matrix is the most widely used method for satellite image classification. Generally, the relation between the reference data and the corresponding result of the classification is compared in a confusion matrix. Many measures of accuracy assessment such as overall accuracy, errors of omission, errors of commission, user's accuracy, producer's accuracy, kappa statistics, and fuzzy accuracy can be evaluated from the confusion matrix. In our study, we assessed the classification's accuracy with the calculation of overall accuracy, producer's accuracy, user's accuracy, and kappa statistics.

The overall accuracy of the classifier can be evaluated by dividing the total number of correctly classified pixels by the total number of reference pixels. The user's accuracy, precision, is the number of correctly classified pixels in each category divided by the total row for that class. The producer's accuracy, recall, is calculated by dividing the number of correctly classified pixels in each category (on the major diagonal) divided by the number of test set pixels used for that category (the column total). The kappa statistic is computed using the following formula:

$$\hat{k} = \frac{N\sum_{i=1}^{r} x_{ii} - \sum_{i=1}^{r}(x_{i+}\cdot x_{+i})}{N^2 - \sum_{i=1}^{r}(x_{i+}\cdot x_{+i})} \quad (7)$$

where:

r = number of rows in the error matrix

x_{ii} = number of observations in row I and column i

x_{i+} = total number of observations in row i

x_{+i} = total number of observations in column i

N = total number of observations included in matrix

CHAPTER 4
EXPERIMENT IMPLEMENTATION, RESULT, AND DISCUSSION

4.1 Land Cover Classification of Landsat TM and ETM+

In this experiment, land cover classification is performed based on the training data extracted using QGIS semi-automatic plugin. The study approach is to detect change of land cover using time series satellite images and land cover classification from 1987 to 2012 is investigated. During those years, only Landsat images are available for research purposes of the study area, and there is no ground-truth observation. Thus, Landsat TM and ETM+ images are used for land cover classification for the past 25 years.

First, image pre-processing of TM and ETM+ images are performed on GEE to achieve an enhanced image for feature extraction. Feature extraction is carried out based on the NDVI values of each land cover class. NDVI values in the study area are divided into seven ranges for the image and training data are extracted for each year. For satellite images, which will be classified on GEE, NDVI, NDBI, and SRTM slopes are combined to those images by layer stacking technique. The red, green, blue and NIR bands are assigned as input values in RF classifier.

When satellite images of the whole year are used in this experiment, those images may be affected by atmospheric interferences during the rainy season. The accessed period of satellite images, sometimes called the temporal feature, is defined between January and May. This is because the weather for these 5 months is mostly clear in the study area. Landsat 5 TM images are used for land cover classification in 1987, and the output classification map is shown in Figure 4.1 (a). The land cover is categorized into seven classes: shrubland, bare land, agriculture, forest, build up, river, and lake. The accuracy assessment of land cover classification in 1987 is conducted as discussed in Section 3.7.

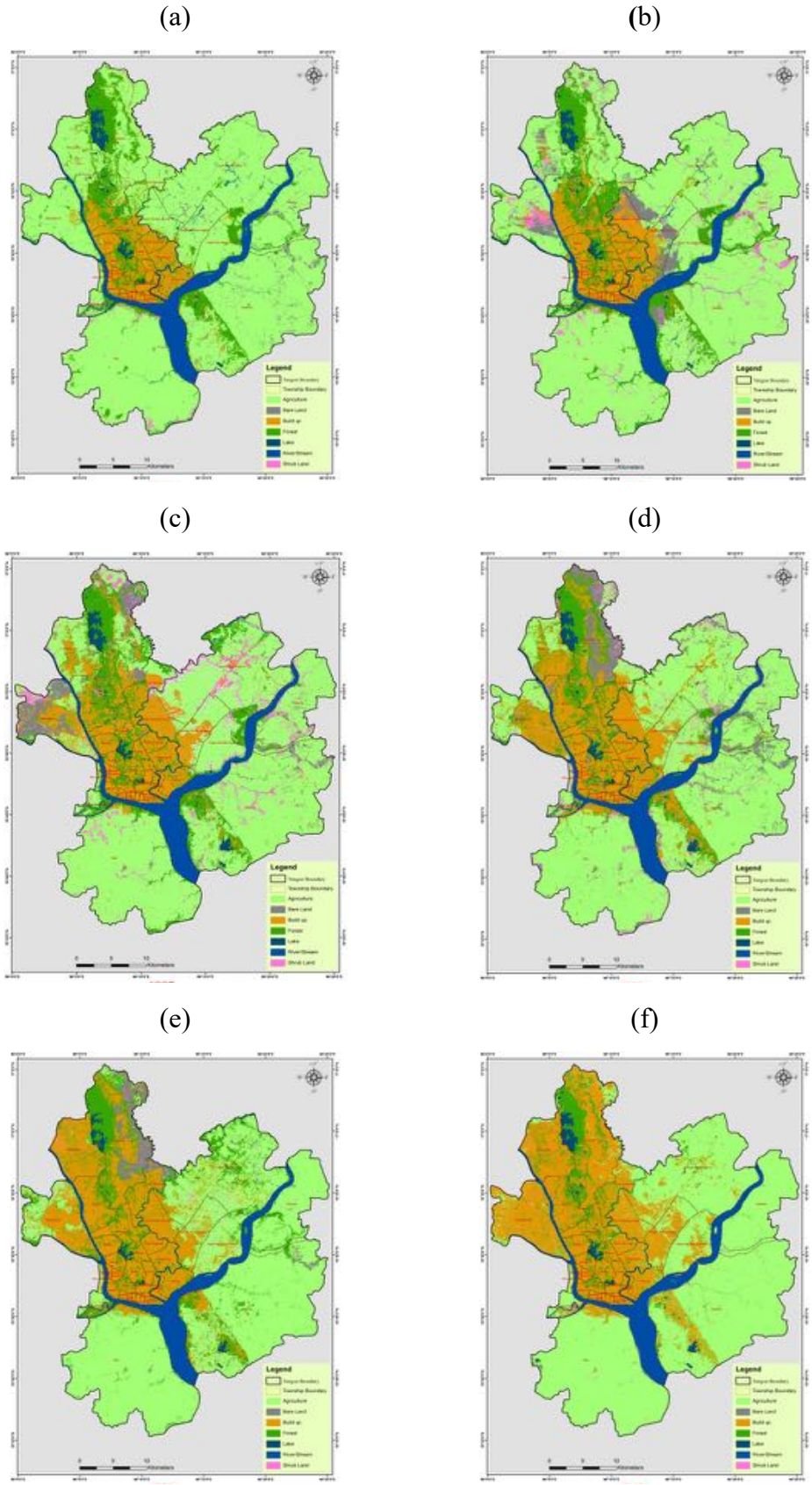

Figure 4.1. Land Cover Map of Yangon in (a)1987 (b)1992 (c)1997 (d)2002 (e) 2007 (f) 2012

Table 4.1 shows the results obtained from the classified map of 1987. The overall accuracy is 88.03% and the kappa statistics is 0.84. The shrubland results in the lowest producer's and user's accuracy with 46.66% and 63.99% respectively. River and lake classifications are well performed with 96.10 % of producer's accuracy and 96.14% of user's accuracy in 1987.

Table 4.1 Classification Accuracy obtained by RF in 1987

Classes	Producer's Accuracy (%)	User's Accuracy (%)
Shrub Land	46.66	63.99
Bare Land	82.15	85.52
Forest	87.75	83.02
Agriculture	88.46	85.77
Build Up	83.63	79.21
Lake	95.72	96.14
River	96.10	94.66
Overall Accuracy		88.03 %
Kappa Statistics		0.84

Table 4.2 Classification Accuracy obtained by RF in 1992

Classes	Producer's Accuracy (%)	User's Accuracy (%)
Shrub Land	71.49	69.77
Bare Land	79.79	80.13
Forest	96.95	96.60
Agriculture	89.54	90.04
Build Up	89.68	89.96
Lake	99.56	99.70
River	99.79	99.74
Overall Accuracy		92.85 %
Kappa Statistics		0.91

The classifications and accuracy assessments of other five years are also investigated as the classification in 1987. Landsat 5 TM images are used for the classifications in 1992 and 1997. The classifications in 2002, 2007 and 2012 are performed using data from Landsat 7 ETM^{+}. Figure 4.1 shows land cover classification map of Yangon generated by RF model for six years.

Table 4.3 Classification Accuracy obtained by RF in 1997

Classes	Producer's Accuracy (%)	User's Accuracy (%)
Shrub Land	70.54	70.45
Bare Land	75.07	75.07
Forest	87.56	87.28
Agriculture	86.87	87.24
Build Up	87.22	86.56
Lake	99.10	99.22
River	99.94	99.94
Overall Accuracy		90.50 %
Kappa Statistics		0.88

Table 4.4 Classification Accuracy obtained by RF in 2002

Classes	Producer's Accuracy (%)	User's Accuracy (%)
Shrub Land	71.01	69.05
Bare Land	74.58	73.11
Forest	89.10	89.28
Agriculture	85.94	86.59
Build Up	91.27	91.42
Lake	99.17	99.25
River	99.98	99.95
Overall Accuracy		91.87 %
Kappa Statistics		0.90

Table 4.5 Classification Accuracy obtained by RF in 2007

Classes	Producer's Accuracy (%)	User's Accuracy (%)
Shrub Land	64.48	66.70
Bare Land	71.59	66.07
Forest	82.19	83.24
Agriculture	83.21	82.34
Build Up	88.35	90.40
Lake	97.62	97.40
River	98.32	97.98
Overall Accuracy		86.80 %
Kappa Statistics		0.84

Table 4.6 Classification Accuracy obtained by RF in 2012

Classes	Producer's Accuracy (%)	User's Accuracy (%)
Shrub Land	82.67	78.45
Bare Land	75.01	73.93
Forest	88.54	88.14
Agriculture	89.41	88.97
Build Up	92.71	94.40
Lake	97.70	99.03
River	98.50	99.19
Overall Accuracy		90.07 %
Kappa Statistics		0.87

The accuracy assessment of each year is calculated using overall accuracy, kappa statistic, producer's accuracy, and user's accuracy in Table 4.2, 4.3, 4.4, 4.5 and 4.6 respectively. Among them, the classification in 1992 achieves the highest overall accuracy of 92.85% and kappa value of 0.91.

4.2 Land Cover Classification of 2017 Data

Landsat 8 and Sentinel 2 data are available for 2017 and the classification is performed using features from these two satellites. Furthermore, open social data from OSM and GPS data from field survey are also used in the contribution of the proposed approach.

4.2.1 Classification using Combination of Pixel and Object-based Approach

The training data for this experiment are collected by combining vector features from Landsat OLI and Sentinel MSI images. The integrated method of pixel-based classification and object-based segmentation for land cover mapping is proposed to achieve a better result. In pixel-based approach, the vector extraction is performed with the spatial and spectral features of the cells of a raster. Six land cover categories (Waterbody, Bare land, Shrubland, Agriculture, Forest, and Build up) are classified from the colour composite of Landsat 8 image. Seven land cover categories (Bare land, Shrubland, Agriculture, Forest, Build up, River, and Lake) with spatial, spectral, and temporal features are extracted from Sentinel 2 image using object-based segmentation method.

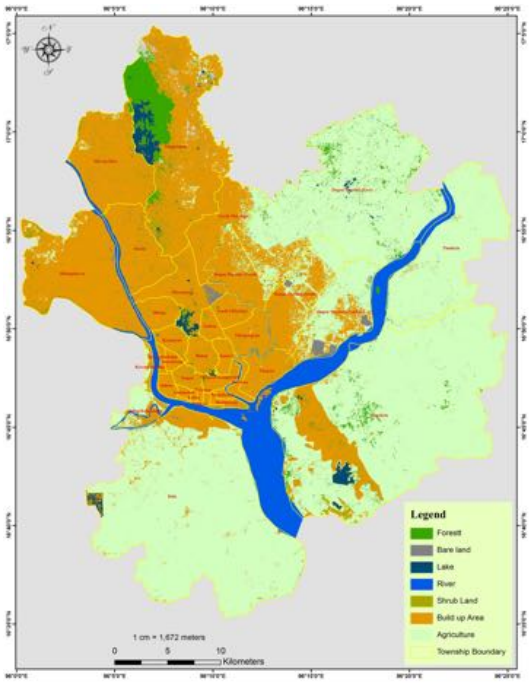

Figure 4.2. Land Cover Map of Yangon in 2017 generated by RF using the Combination of Pixel and Object-based approaches

There are total 7378 vectors in the dataset. 60% of dataset are used for training and 40% are used for testing. The satellite image fusion is performed by stacking of 4 bands (Red, Green, Blue, and NIR) from Landsat 8 with 4 bands (Red, Green, Blue, and NIR) from Sentinel 2. Furthermore, NDVI and NDBI spectral indexes calculated from those two satellites and SRTM slopes are also added to input image. There are total 13 bands. The classification is deployed on GEE and the classification accuracy is described in Table 4.7. The model generates land cover classification map of Yangon in 2017, as shown in in Figure 4.2. The overall accuracy of 95.62% and kappa statistic of 0.92 are obtained using a combination of pixel and object-based approaches.

Table 4.7 Classification Accuracy obtained by RF using the Combination of Pixel and Object-based approaches in 2017

Classes	Producer's Accuracy (%)	User's Accuracy (%)
Shrub Land	51.70	52.24
Bare Land	80	76.83
Forest	90.92	92.77
Agriculture	96.89	96.81
Build Up	93.62	92.96
Lake	98.17	98.41
River	98.53	98.62
Overall Accuracy		95.62 %
Kappa Statistics		0.92

4.2.2 Classification using Open Social Data

The open social data from OSM and GPS metadata are combined to the previous dataset in this experiment. The vector layers from OSM map are rasterized to a 5-m grid that is superimposable with the satellite images. The total 7813 vectors of dataset are trained in RF model. Classification that uses spectral bands as the input parameter becomes one of the constitutional arguments. Thus, different spectral bands combination is investigated in RF classifier.

Table 4.8 Summary of Classification Accuracies based on the Input Bands Combination of RF in 2017

No.	Spectral Wavelength Used in Classification	Overall Accuracy	Kappa Statistics
1.	Landsat8 B2,B3,B4,B5,B6 and Sentinel B2,B3,B4,B8	96.19%	0.94
2.	Landsat8 B2,B3,B4,B5,B6 and Sentinel B2,B3,B4,B8,B11	96.25%	0.95
3.	Landsat8 B2,B3,B4,B5,B6,B9 and Sentinel B2,B3,B4,B8,B11	96.19%	0.94
4.	Landsat8 B2,B3,B4 and Sentinel B2,B3,B4	94.44%	0.92
5.	Landsat8 B2,B3,B4,B5 and Sentinel B2,B3,B4,B8	95.33%	0.93
6.	Landsat8 B1,B2,B3,B4,B5,B6,B9 and Sentinel B1,B2,B3,B4,B8,B10,B11	96.71%	0.951
7.	Landsat8 B1,B2,B3,B4,B5,B6 and Sentinel B1,B2,B3,B4,B8,B11	96.73%	0.952

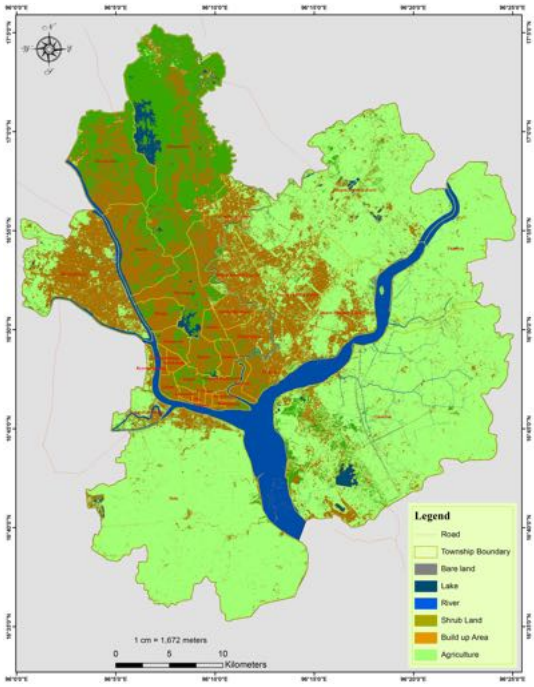

Figure 4.3. Land Cover Map of Yangon in 2017 generated by RF using the Features from Pixel, Object-based, GPS metadata, and OSM

Table 4.8 describes the summary classification accuracies obtained from RF based on the input spectral bands combination 2017. The combination of B1, B2, B3, B4, B5, B6 from Landsat 8 and B1, B2, B3, B4, B8, B11 from Sentinel 2 obtains highest overall accuracy of 96.73% followed by kappa statistic of 0.952. The detailed precision and recall for each land cover classes based on band combination are described in Table 4.9. River and lake classes are more correctly classified than others. Figure 4.3 shows land cover map of Yangon in 2017 obtained from the proposed approach.

Table 4.9 Classification Accuracy obtained by RF using the Features from Pixel, Object-based, GPS metadata, and OSM in 2017

Classes	Producer's Accuracy (%)	User's Accuracy (%)
Shrub Land	59.05	60.17
Bare Land	78.99	81.71
Forest	97.19	97.23
Agriculture	96.72	97.21
Build Up	96.51	95.52
Lake	98.86	99.16
River	99.25	99.38
Overall Accuracy		96.73 %
Kappa Statistics		0.95

4.3 Comparison of Classifications using Different GEE Classifiers

The proposed experiment aims to analyse land cover classification using GEE six machine learning classifiers and compares their accuracies. Land cover classifications of study area in 2017 are investigated by using RF, CART, Multiclass Perceptron, GMO Max Entropy, Minimum Distance, and Continuous Naïve Bayes algorithms. The summary accuracy assessments for all classifications are described in Table 4.10. Figure 4.4 shows classification maps of Yangon obtained using six classifiers in GEE.

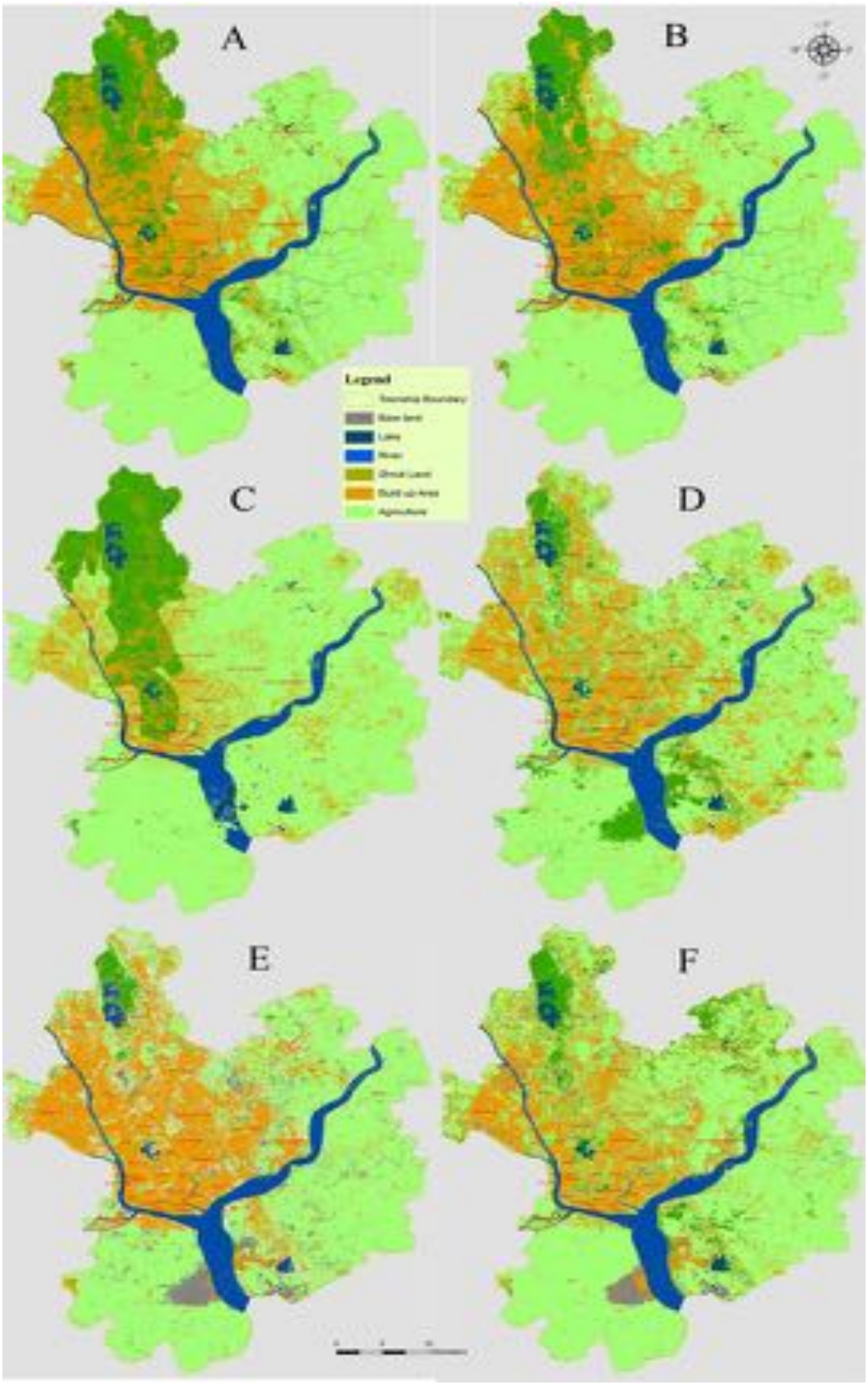

Figure 4.4. Land cover maps of Yangon in 2017 generated by (A) RF, (B) CART, (C) Multiclass Perceptron, (D) GMO Max Entropy, (E) Minimum Distance and (F) Continuous Naïve Bayes algorithms

RF and CART achieve overall accuracies of 96.73% and 95.09% and kappa statistics of 0.952 and 0.927. Multiclass perceptron classifier is trained with 65 epochs and 66.21% overall accuracy and 0.437 kappa statistic is obtained. GMO max entropy and continuous naïve Bayes result overall accuracy of 80.85% and 81.53%, and kappa statistics of 0.716 and 0.733 respectively. Minimum distance algorithm is implemented based on the Mahalanobic distance value from the class's mean, and overall accuracy of 87.85% and kappa statistic of 0.827 is achieved. Based on the results from Table 4.10, the decision tree-based classifiers such as RF and CART outperformed than other classifiers, and multiclass perceptron produces the lowest accuracy of 66.21%.

Table 4.10 Summary of Overall classification accuracies and kappa statistics achieved by GEE machine learning classifiers

Classifier	Overall Accuracy (%)	Kappa Statistics
Random Forest	96.73	0.952
CART	95.09	0.927
Multiclass Perceptron	66.21	0.437
GMO Max Entropy	80.85	0.716
Minimum Distance	87.85	0.827
Continuous Naïve Bayes	81.53	0.733

4.4 Post-Classification Change Detection using Time Series Data

In this section, change detection of Yangon for 30years is implemented using PCC approach in QGIS. Change detection is performed based on the previous classification results of time series data. Change detection results are shown in thematic map and the legend in map identifies changes from one class to another. For clear visualization of changes, land cover change map for each 5years interval is investigated. The overall change detection map from 1987 to 2017 is also generated as shown in Figure 4.11. Land cover change maps of 1987-1992, 1992-1997, 1997-2002, 2002-2007, 2007-2012, and 2012-2017 are shown in Figure 4.5, 4.6, 4.7, 4.8, 4.9, and 4.10 respectively.

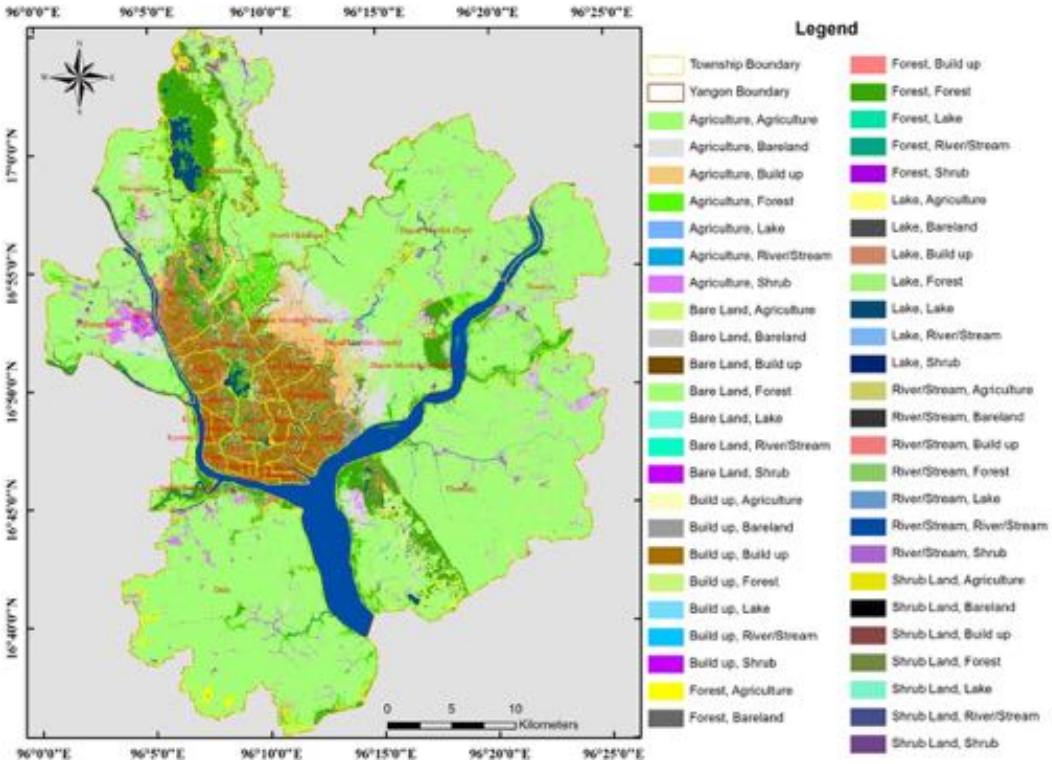

Figure 4.5. Thematic map of LCCD from 1987 to 1992 in Yangon

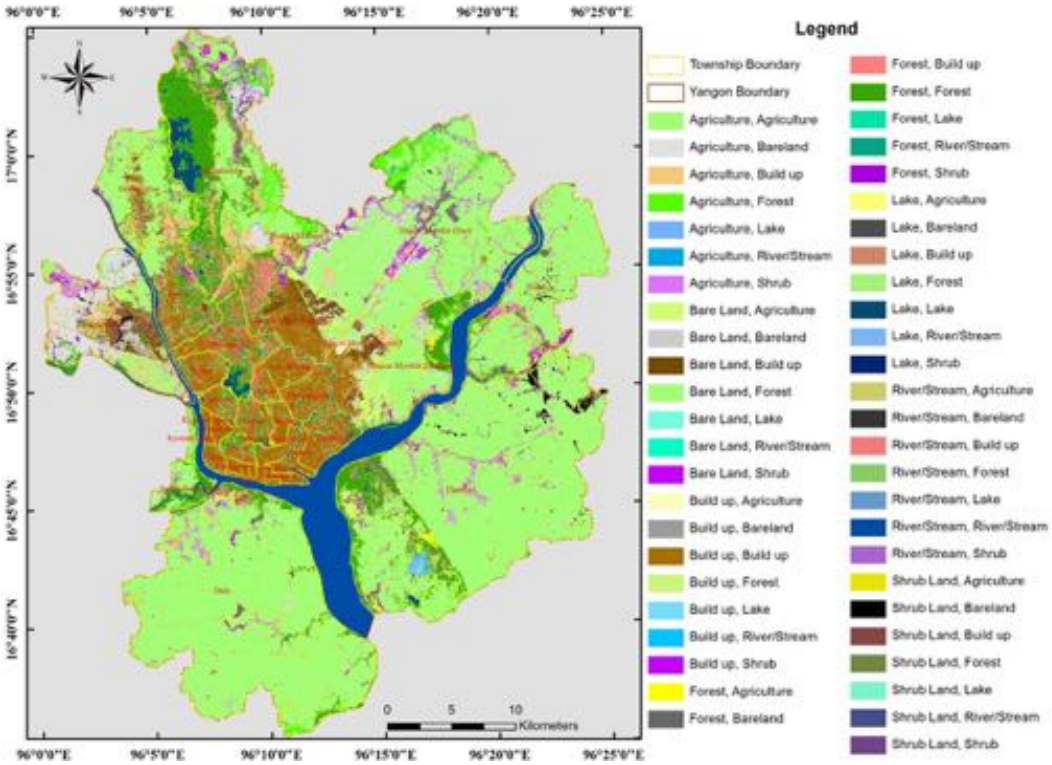

Figure 4.6. Thematic map of LCCD from 1992 to 1997 in Yangon

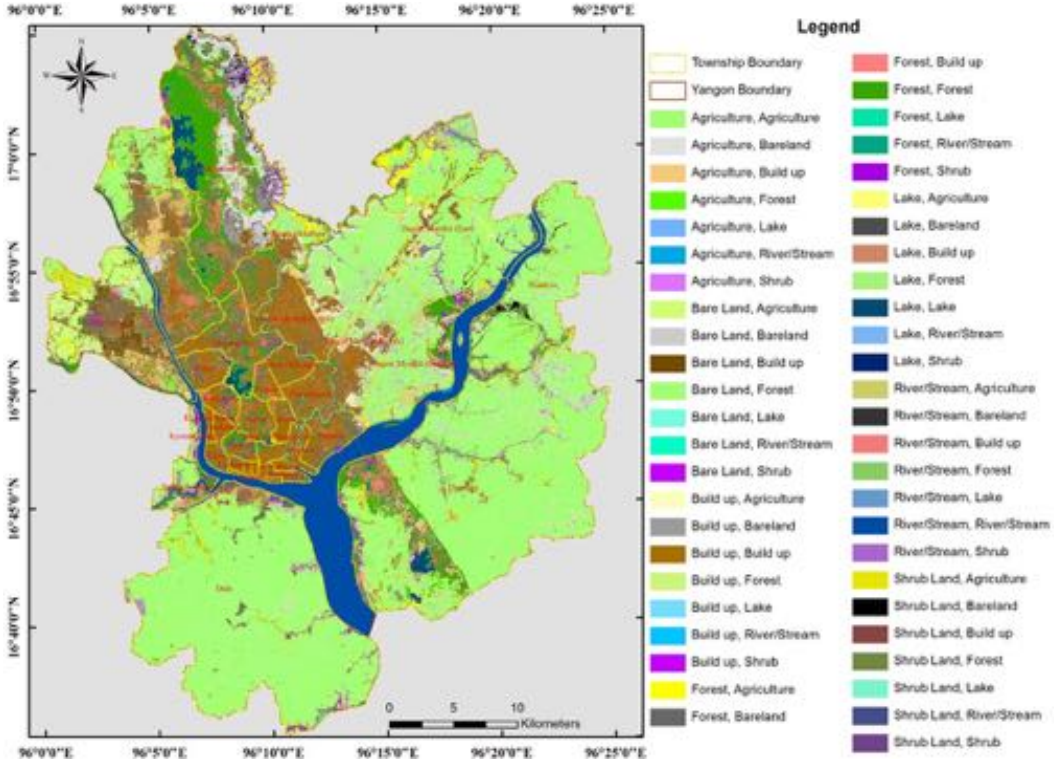

Figure 4.7. Thematic map of LCCD from 1997 to 2002 in Yangon

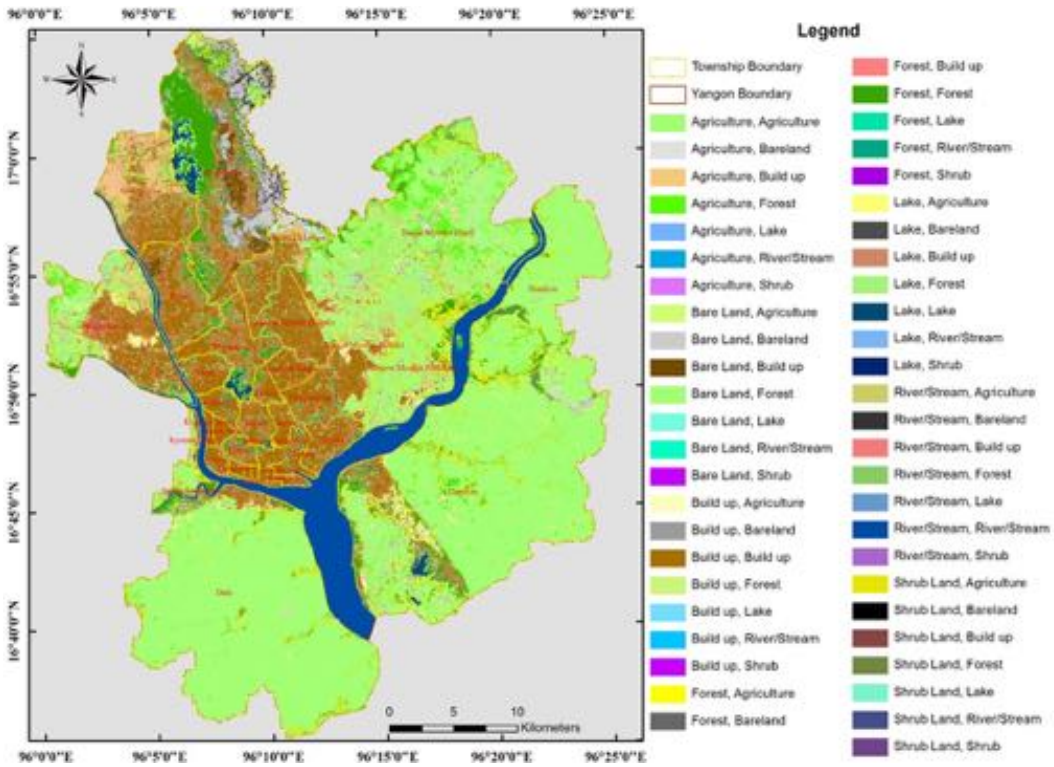

Figure 4.8. Thematic map of LCCD from 2002 to 2007 in Yangon

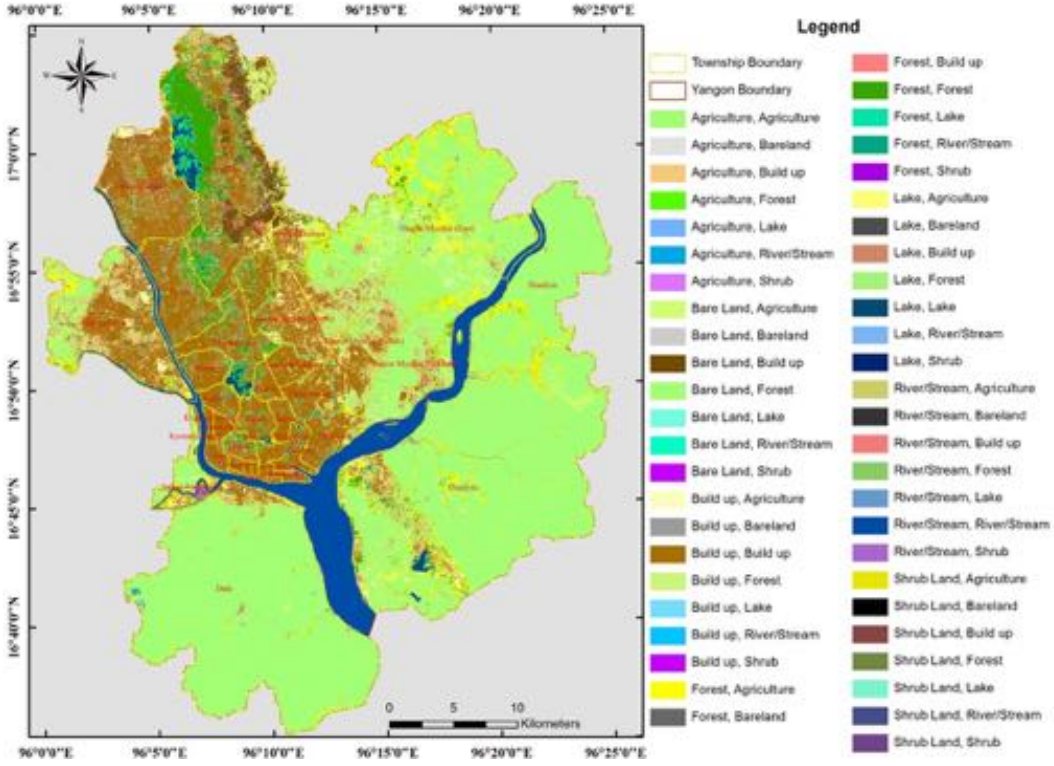

Figure 4.9. Thematic map of LCCD from 2007 to 2012 in Yangon

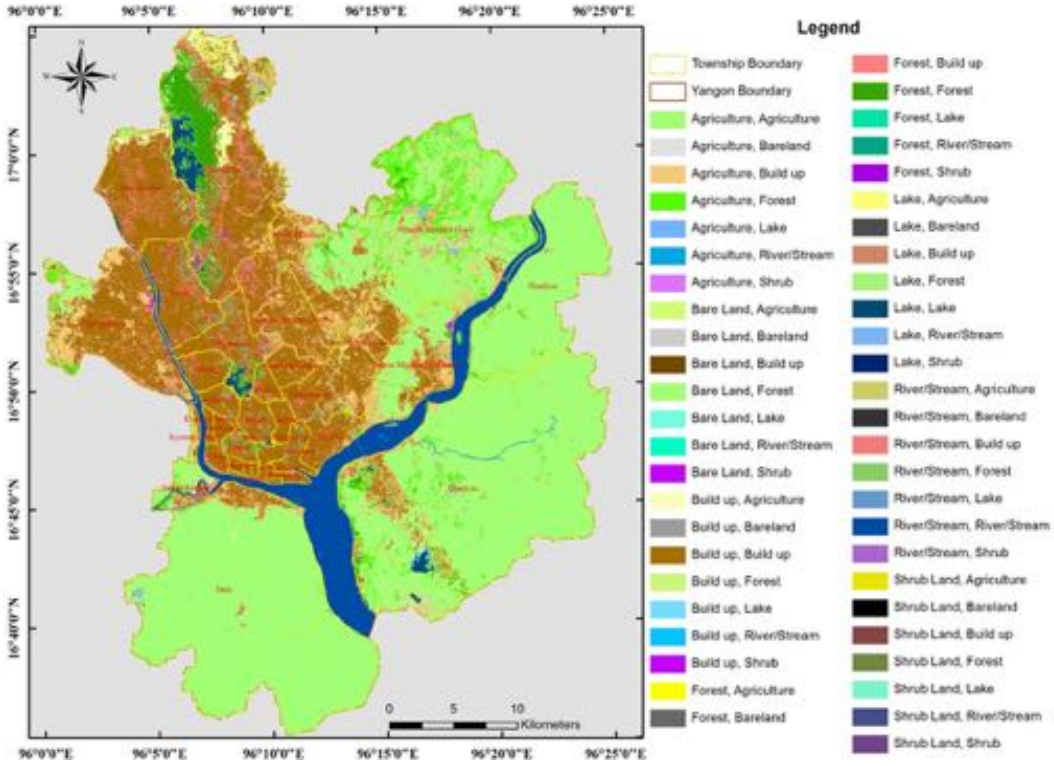

Figure 4.10. Thematic map of LCCD from 2012 to 2017 in Yangon

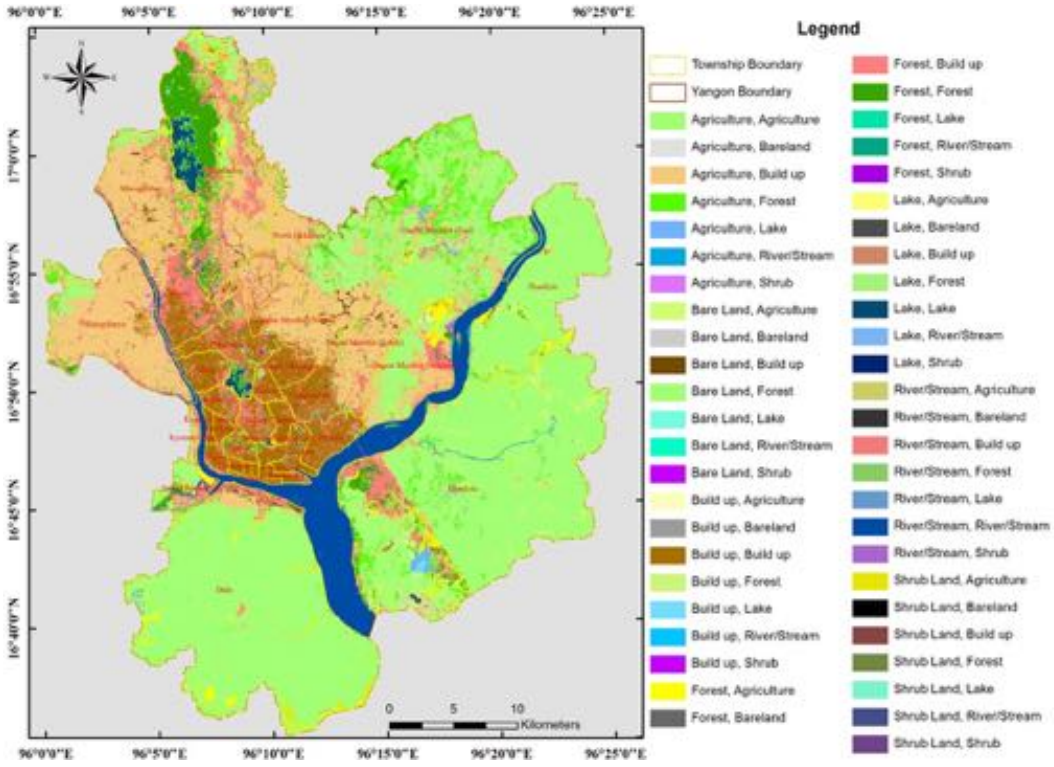

Figure 4.11. Thematic map of LCCD from 1987 to 2017 in Yangon

Area coverage of land cover in the study area is calculated in terms of square kilometres using classified map, and the results are described in the following Table 4.11. The bar chart of Figure 4.12 shows comparison of land cover coverage in seven classes for 30 years.

Table 4.11 Area Coverage of each Land Cover Classes from 1987 to 2017 in km^2

Classes	Y_1987	Y_1992	Y_1997	Y_2002	Y_2007	Y_2012	Y_2017
Agriculture	969.4	860.259	747.048	731.063	729.75	829.334	767.804
Bare Land	30.7707	53.789	61.8264	65.3149	41.9371	7.71521	0.018353
Build up	114.258	137.323	218.509	263.099	315.889	351.436	333.956
Forest	166.146	175.434	187.106	176.372	201.819	116.267	168.995
Lake	18.43495	15.5275	16.4128	17.822	10.9388	20.5083	15.2694
River	99.0841	103.474	99.1864	97.3315	96.7807	98.4398	101.454
Shrub Land	7.21838	59.5037	67.0314	54.3191	9.59974	8.41405	5.21174

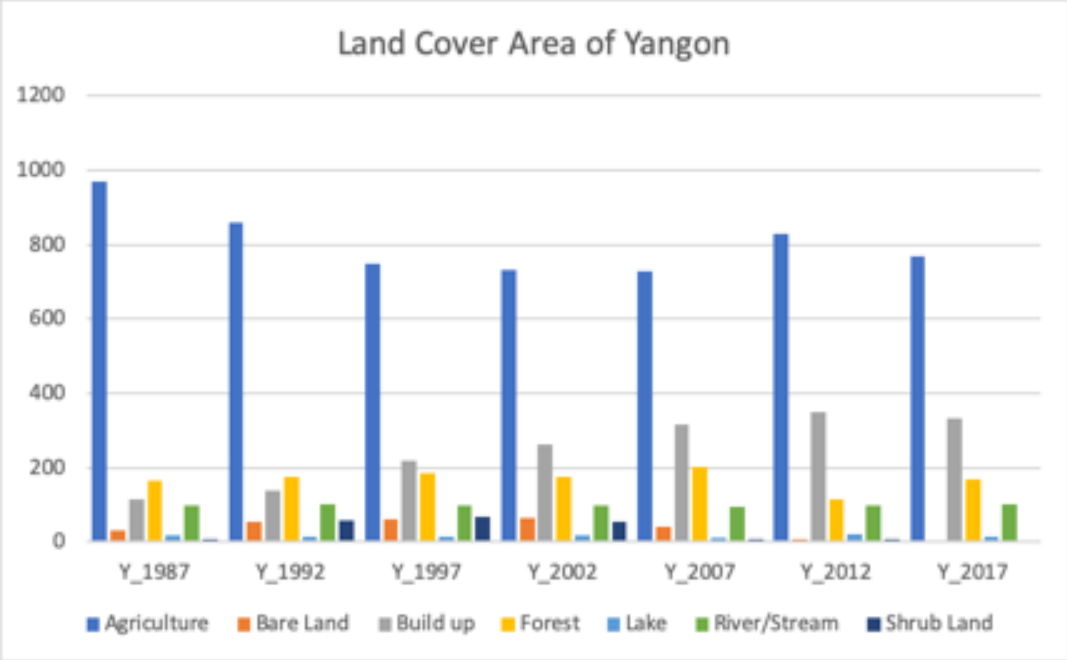

Figure 4.12. Chart of area coverage of each land cover classes by km^2 in seven years

The percentage values of each land cover area coverage is also calculated as shown in Table 4.12. The line chart that describes how land cover classes are decreased or increased year by year using percent values is showns in Figure 4.13 for the dramatic changes.

Table 4.12 Area Coverage of Land Cover in term of percentages for all classes from 1987 to 2017

Types	Y_1987	Y_1992	Y_1997	Y_2002	Y_2007	Y_2012	Y_2017
Agriculture	68.98	61.21	53.47	52.02	51.88	58.96	55.13
Bare Land	2.19	3.83	4.43	4.65	2.98	0.55	0
Build up	8.13	9.77	15.64	18.72	22.46	23.18	23.98
Forest	11.82	12.48	13.39	12.55	14.35	8.27	12.13
Lake	1.31	1.10	1.17	1.27	0.78	1.46	1.10
River	7.05	7.36	7.10	6.93	6.88	7.00	7.28
Shrub Land	0.51	4.23	4.80	3.87	0.68	0.60	0.37

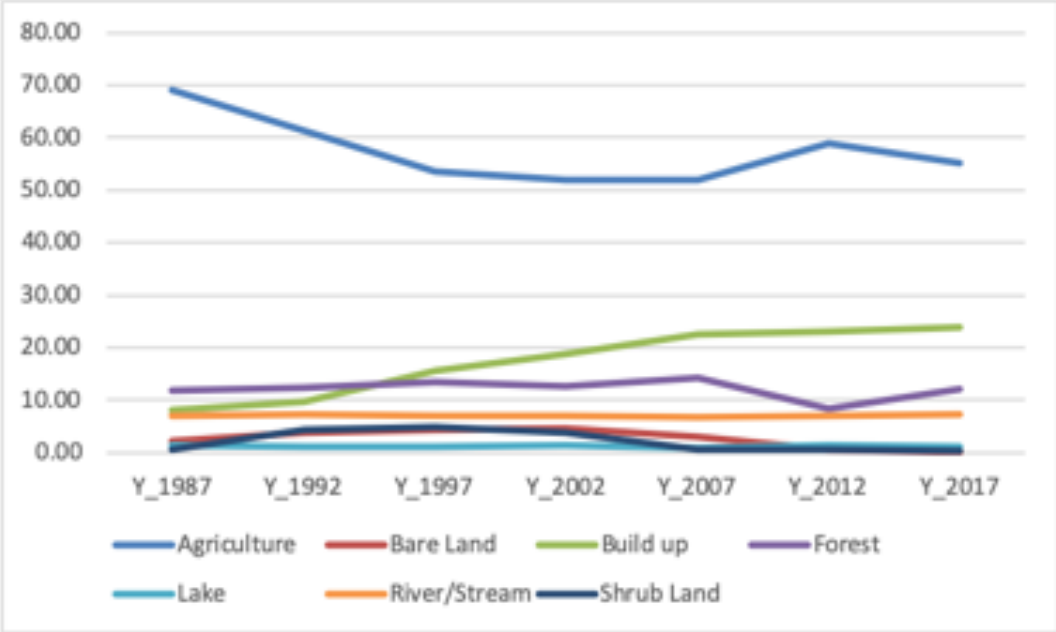

Figure 4.13 Land Cover Change for each class between 1987 and 2017

4.5 Summary

This chapter describes the system implementation of the proposed approach using time series data of satellites with detailed procedures. The classified map and accuracy assessment are identified for each experiment and change detection is also demonstrated with the thematic map, bar chart, and line chart.

CHAPTER 5
CONCLUSION AND FUTURE WORK

5.1 Conclusion

Land cover mapping and change detection using RS and GIS provide valuable and effective information for developing country infrastructure. Accurate and reliable land resources can build a sustainable developed country and this research aims to achieve this goal. Based on the experimental results described in Chapter 4, the proposed approach is feasible to provide information to national decision makers.

The obtained result shows that significant changes have occurred in land cover, particularly in agriculture, bare land, and build up area in the past thirty years. The research contributes to the land cover application of cloud computing engine GEE and its potential for the environmental research. The overall thesis is conducted by combining features from the pixel, object-based approaches, and by performing OSM and PCC to generate a changing trend. Feature levels fusion of different satellite sensors can improve classification accuracy. Furthermore, the spectral index also serves as an important feature when considering classification. The combination of input band classifier has shown significant improvement in accuracy, and it also participates as an effective matter.

In conclusion, time series analysis of satellite images for change detection contributes to the quantification and understanding the surface changes on the earth. Moreover, the utilization of cloud-based engines in urban and environmental monitoring becomes useful roles due to their computing time, speed and cost. Machine learning classifiers and satellite images can help the environment and human society based on the effective investigation in real-world problems.

5.2 Future Work

Detection of land cover change is an important issue in most land remote sensing and urban planning communities. Efficient and accurate land resources can be obtained based on artificial intelligent algorithms that run on high- resolution images. Although this study demonstrates effective change detection and the classified map with high accuracy, their application in real urban planning

environment is limited. Only seven land cover classes are classified by this approach. This study can be extended to land use land cover monitoring if the reliable ground truth data and high resolution images are obtained. High resolution images can be acquired using drone and satellite orbiting near the surface of the earth.

From a machine learning perspective, parameter tuning of machine learning can improve classifier performance and accuracy. Furthermore, the analysis of land use land cover from high-resolution images can be performed not only the use of machine learning classifiers but also the use of deep learning classifiers. The dataset of land use land cover studies for the wide area will be enormous. Thus, deep learning methods may perform better than machine learning for huge data.

REFERENCES

[1] Ministry of Immigration and Population. (2015): The Union Report: Census Report. The 2014 Myanmar Population and Housing Census vol.2. [Online]. Available at. http://www.burmalibrary.org/docs22/2014-Census-Volume 2C- Religion-red.pdf. Accessed date: May 30, 2019.

[2] JICA and YCDC (Japan International Corporation Agency and Yangon City Development Committee). (2014): A Strategic Urban Development Plan of the Greater Yangon: Final Report II Summary. [Online]. Available at. http://open_jicareport.jica.go.jp/pdf/12145975.pdf. Accessed date: Oct 25, 2017.

[3] D. Phiri, J. Morgenroth, "Developments in Landsat Land Cover Classification Methods: A Review," Remote Sens. 2017, vol. 9, 967; doi:10.3390/rs9090967, Sep 19, 2017.

[4] B. Chen, B. Huang, B. Xu, "Multi-source remotely sensed data fusion for improving land cover classification," ISPRS Journal of Photogrammetry and Remote Sensing, Vol. 124, pp. 27-39, Dec 29, 2016.

[5] W. B. Meyer, "Past and Present Land Use and Land Cover in the USA," Consequences 1995, vol. 1(1), pp. 24-33.

[6] E. Ellis. Land-use and land-cover change. *The Encyclopedia of Earth*. [Online] Available at. https://editors.eol.org/eoearth/wiki/Land-use_and_ land-cover_change. Accessed date: Jun 13, 2019.

[7] European Commission. (2001): Manual of concepts on land cover and land use information systems. p. 106. Luxembourg.

[8] H. Keshtkar, W. Voigt, " A spatiotemporal analysis of landscape change using an integrated Markov chain and cellular automata models," Model. Earth Syst. Environ. (2016) 2:1-13, doi.org/10.1007/s40808-015-0068-4, March 2016.

[9] Y. Zhao, M. Tomita, K. Hara, M. Fujihara, Y. C. Yang, L. J. Da, "Effects of topography on status and changes in land-cover patterns, Chongqing City, China," Landscape Ecol. Eng. (2014), Vol.10(1), pp. 125-135, doi.org/10. 1007/s11355-011-0155-2, Jan 2014.

[10] T. M. Lillesand, R. W. Kiefer, J. W. Chipman. (2015): Remote Sensing and Image Interpretation, Seventh edition. United States of America: John Wiley & Sons.

[11] Canada Centre of Remote Sensing. (2007): Fundamentals of Remote Sensing.[Online]. Available at. https://www.nrcan.gc.ca/sites/www.nrcan.gc.ca/files/earthsciences/pdf/resource/tutor/fundam/pdf/fundamentals_e.pdf. Accessed date: Jun 16, 2019.

[12] J. R. Jensen. (2015): Introductory Digital Image Processing: A Remote Sensing Perspective, Fourth edition. United States of America: Pearson Education.

[13] D. Faggella. What is Machine Learning?. (2019). [Online]. Available at. https://emerj.com/ai-glossary-terms/what-is-machine-learning/. Accessed date: Jun 16, 2019.

[14] M. Mohri, A. Rostamizadeh, A. Talwalkar. (2012): Foundations of Machine Learning. London, England: Massachusetts Institute of Technology.

[15] T. O. Ayodele. (2010): Types of Machine Learning Algorithms, New Advances in Machine Learning, Yagang Zhang (Ed.), ISBN: 978-953-307-034-6, InTech, [Online] Available at. https://www.intechopen.com/books/new-advances-in-machine-learning/types-of-machine-learning-algorithms. pp. 19-24. Accessed date: Jun 16, 2019.

[16] J. Brownlee. (2016): Master Machine Learning Algorithms: Discover How They Work and Implement Them from Scratch. [Online]. Available at. https://machinelearningmastery.com/master-machine-learning-algorithms/. Accessed date: Dec 7, 2018.

[17] M. Sanjeevi. Different Types of Machine Learning and their types. Sep 26 2017. [Online]. Available at. https://medium.com/deep-math-machine-learning-ai/different-types-of-machine-learning-and-their-types-34760b9128a2. Accessed date: Jun 16, 2019.

[18] P. Bajaj. Reinforcement Learning. [Online]. Available at. https://www.geeksforgeeks.org/what-is-reinforcement-learning/. Accessed date: Jun 16, 2019.

[19] A. Singh, “Digital Change Detection Techniques using remotely-sensed data,” International Journal of Remote Sensing, 1989, Vol.10(6), pp. 989-1003.

[20] D. Lu, P. Mausel, E. Brondizio, E. Moran, “Change Detection Techniques,” International Journal of Remote Sensing, 2004, Vol.25(12), pp. 2365-2401.

[21] R. Jhonnerie, V. P. Siregar, B. Nababan, L. B. Prasetyo, S. Wouthuyzen, “Random forest classification for mangrove land cover mapping using Landsat 5 TM and ALOS PALSAR imageries,” The 1st Int. Symposium on LAPAN-IPB Satellite for Food Security and Environmental Monitoring, Procedia Environmental Sciences (2015), Vol.24, pp. 215-221.

[22] Y. H. Tsai, D. Stow, H. L. Chen, R. Lewison, L. An, L. Shi, “Mapping Vegetation and Land Use Types in Fanjingshan National Nature Reserve Using Google Earth Engine,” Remote Sens. 2018, 10, 927; doi:10.3390/ rs10060927, Jun 12, 2018.

[23] U. Pimple, D. Simonetti, A. Sitthi, S. Pungkul, K. Leadprathom, H. Skupek, J. Som-ard, V. Gond, S. Towprayoon, “Google Earth Engine Based Three Decadal Landsat Imagery Analysis for Mapping of Mangrove Forests and Its Surroundings in the Trat Province of Thailand,” Journal of Computer and Communications, 6, pp. 247-264, Dec 29, 2017, DOI: 10.4236/jcc.2018.61025.

[24] G. T. Ayele, A. K. Tebeje, S. S. Demissie, M. A. Belete, M. A. Jemberrie, W. M. Teshome, D. T. Mengistu, E. Z. Teshale, “Time Series Land Cover Mapping and Change Detection Analysis Using Geographic Information System and Remote Sensing, Northern Ethiopia,” Air, Soil and Water Research (2017), Vol.11, pp. 1-18, https://doi.org/10.1177%2F1178622117751603.

[25] A. Midekisa, F. Holl, D. J. Savory, R. A. Pacheco, P. W. Gething, A. Bennett, H. J. W. Sturrock, “Mapping land cover change over continental Africa using Landsat and Google Earth Engine cloud computing,” PLoS ONE 12 (9): e0184926, Sep 27, 2017, https://doi.org/10.1371/journal.pone.0184926.

[26] A. Shelestov, M. Lavreniuk, N. Kussul, A. Novikov, S. Skakun, " Exploring Google Earth Engine Platform for Big Data Processing: Classification of Multi-Temporal Satellite Imagery for Crop Mapping," Front. Earth Sci. 5:17, Feb 24, 2017, https://doi.org/10.3389/feart.2017.00017.

[27] J. Xiong, P. S. Thenkabail, J. C. Tilton, M. K. Gumma, P. Teluguntla, A. Oliphant, R. G. Congalton, K. Yadav, N. Gorelick, "Nominal 30-m Cropland Extent Map of Continental Africa by Integrating Pixel-Based and Object-Based Algorithms Using Sentinel-2 and Landsat-8 Data on Google Earth Engine," *Remote Sensing*. 2017; 9(10):1065, Oct 19, 2017, https://doi.org/10.3390/rs9101065.

[28] T. Sritarapipat, W. Takeuchi, "Urban Growth Modelling based on the Multi-centres of the Urban Areas and Land Cover Change in Yangon, Myanmar," Journal of the Remote Sensing Society of Japan, Vol. 37, No. 3(2017), pp. 248-260.

[29] Y. Wang, B. K.H. Hu, S. W. Myint, C. Feng, W. T.L. Chow, P. F. Passy, "Patterns of land change and their potential impacts on land surface temperature change in Yangon, Myanmar," Science of the Total Environment, Vol.643, pp. 738-750, Dec 1, 2018, https://doi.org/10.1016/j.scitotenv.2018.06.209.

[30] United States Geological Survey (USGS). Landsat 5. [Online]. Available at. https://www.usgs.gov/land-resources/nli/landsat/landsat-5?qt-science_support__page_related_con=0#qt-science_support_page_related_con. Accessed date: Jun 13, 2019.

[31] United States Geological Survey (USGS). Landsat 7. [Online]. Available at. https://www.usgs.gov/land-resources/nli/landsat/landsat-7?qt-science_support_page_related_con=0#qt-science_support_page_related_con. Accessed date: Jun 18, 2019.

[32] Landsat Science. Landsat 7. [Online]. Available at. https://landsat.gsfc.nasa.gov/landsat-7/. Accessed date: Jun 18, 2019.

[33] United States Geological Survey (USGS). Landsat 8. [Online]. Available at. https://www.usgs.gov/land-resources/nli/landsat/landsat-8?qt-science_supp

ort_page_related_con=0#qt-science_support_page_related_con8. Accessed date: Jun 18, 2019.

[34] Earth Observing System (EOS). Landsat 8. [Online]. Available at. https://eos.com/landsat-8/. Accessed date: Jun 18, 2019.

[35] Sentinel Online. Sentinel 2. [Online]. Available at. https://sentinel.esa.int/web/sentinel/missions/sentinel-2. Accessed date: Jun 18, 2019.

[36] OpenStreetMap Foundation. Open Street Map. [Online]. Available at. https://wiki.osmfoundation.org/wiki/About. Accessed date: Jun 18, 2019.

[37] GPS.GOV. Global Positioning System. [Online]. Available at. https://www.gps.gov/systems/gps/. Accessed date: Jun 20, 2019.

[38] GIS Geography. Normalized Difference Vegetation Index. [Online]. Available at. https://gisgeography.com/ndvi-normalized-difference-vegetation-index/. Accessed date: Jun 20, 2019.

[39] T. G. Farr, P. A. Rosen, E. Caro, R. Crippen, R. Duren, S. Hensley, M. Kobrick, M. Paller, et al., "The Shuttle Radar Topography Mission," Rev. Geophys., 45, RG2004, May 19, 2007, doi:10.1029/2005RG000183.

[40] ENVI. (2008): ENVI Feature Extraction Module User's Guide. ITT Visual Information Solutions.

[41] D. J. Robinson, N. J. Redding, D. J. Crisp, (2002). "Implementation of a fast algorithm for segmenting SAR imagery," Scientific and Technical Report, Jan 1, 2002. Australia: Defense Science and Technology Organization.

[42] N. Horning, "Random Forests: An algorithm for image classification and generation of continuous fields data sets," International Conference on Geoinformatics for Spatial Infrastructure Development in Earth and Allied Sciences, Hanoi, Vietnam, 9-11 Dec 2010.

[43] P. T. Noi, M. Kappas, "Comparison of Random Forest, k-Nearest Neighbor, and Support Vector Machine Classifiers for Land Cover Classification Using Sentinel-2 Imagery," Sensors 2018, Vol.18(18), doi:10.3390/s18010018, Dec 22, 2017.

[44] R. Timofeev to Prof. Dr. W. Hardel, “Classification and Regression Trees (CART). Theory and Applications,” CASE- Centre of Applied Statistics and Economics, Humboldt University, Berlin, Dec 20, 2004.

[45] S. Haykin. (2008): Neural Networks and Learning Machines, 3rd edition. Upper Saddle River: NJ: Prentice Hall.

[46] C. M. Bishop. (2006): Pattern Recognition and Machine Learning. New York, NY: Springer.

[47] E. T. Jaynes, “Information theory and statistical mechanics,” Physical Review, Vol.106(4):620630, 1957.

[48] A. G. Wacker, D. A. Landgrebe, “Minimum Distance Classification in Remote Sensing,” LARS Technical Reports, Paper 25, 1972, [Online]. Available at. https://docs.lib.purdue.edu/larstech/25/, Accessed date: Jun 24, 2019.

LIST OF ACADEMIC ACHIEVEMENT

List of Publications

1. Nyein Soe Thwal, Takaaki Ishikawa, Hiroshi Watanabe: “Land Cover Classification Using Landsat and Sentinel Images y Integrating Pixel and Object-based Segmentation Approach,” Picture Coding Symposium 2018, Image Media Processing Symposium 2018 (PCSJ/IMPS2018), P-2-3, Nov. 2018.
2. Nyein Soe Thwal, Takaaki Ishikawa, Hiroshi Watanabe: “Mapping Urban Land Cover by Using Landsat Sentinel Images and Open Social Data,” 2018 ITE Winter Annual Convention, 22D-4, Dec. 2018.
3. Nyein Soe Thwal, T. Ishikawa, H. Watanabe: “Comparison of Machine Learning Classifiers for Land Cover Mapping in Google Earth Engine,” IEICE General Conference, BS-4-21, Mar. 2019.
4. Nyein Soe Thwal, Takaaki Ishikawa, Hiroshi Watanabe: “Land cover classification and change detection analysis of multispectral satellite images using machine learning,” SPIE. Remote Sensing, Image and Signal Processing for Remote Sensing XXV Conference, Sep. 2019.